Texas A&M University
Mechanical Engineering Department
Turbomachinery Laboratory

Journal Bearing Force Coefficients under High Dynamic Loading – Experimental Results

Research progress Report to the Turbomachinery Research Consortium

by

Luis San Andrés
Professor

TRC-B&C-3-03
May 2003

TRC Project:
Response of a Squeeze Film Damper under High Dynamic Loading and Identification of Damping and Inertia Coefficients

Executive Summary

Lightly damped rotor bearing systems experience large amplitudes of vibration when traversing critical speeds. Traditional fluid film bearing rotordynamic force coefficients, strictly valid for minute motions about an equilibrium position, may not provide reliable predictions for design or trouble shooting in rotordynamics analyses. Experiments assessing the dynamic forced response of a plain journal bearing undergoing large orbital motions due to single-frequency excitation forces were conducted in a test rig. The short test bearing of slenderness ratio L/D=0.25 has a nominal radial clearance of 0.127 mm (5 mils). Tests were conducted at three rotor speeds (900, 1800 and 2700 rpm), three feed pressures (1, 3 and 6 psig), and three excitation frequencies (15, 30 and 45 Hz). Baseline bearing motions due to shaft run-out are recorded and subtracted in the parameter identification procedure. The forces exerted on the bearing induce large orbital motions with peak amplitudes exceeding 50% of the nominal bearing clearance. Analytical direct damping and cross-coupled stiffness coefficients agree favorably with the experimental coefficients, thus demonstrating that linearized force coefficients do fairly well in predicting bearing motions of large amplitude. The bearing whirl frequency ratio approaches the typical 50% value at the highest speed tested. Excitation frequency has a marked influence of the test direct dynamic stiffness coefficients with added mass coefficients at least twice as large as predicted values.

Acknowledgements

Undergraduate student workers, Clinton Adams and Anthony Pruske, prepared the test rig, conducted the experiments and collected the measurements for later analysis by the Principal Investigator. The P.I. thanks the students for their participation in the project.

Table of contents

List of Tables

List of Figures

Nomenclature

$a_{x,y}$	Bearing housing accelerations [m/s^2]
c	Baring radial clearance [0.127 mm – nominal]
$C_{sx,sy}$	Dry (no lubricant) damping coefficients [Ns/m]
$C_{\alpha\beta}$	(Estimated) Bearing damping coefficients [N.s/m], α, β=X,Y
$e_{x,y}$	Bearing static eccentricity [m]
D	Journal Diameter [0.127 m]
$F_{x,y}$	External (shaker) forces applied to bearing [N]
$H_{\alpha\beta}$	$K_{\alpha\beta}+i\omega C_{\alpha\beta}$. Bearing impedance coefficients
i	imaginary unit ($\sqrt{-1}$)
$K_{sx,sy}$	Structural (support) stiffnesses [N/m]
$K_{\alpha\beta}$	(Estimated) Bearing stiffness coefficients [N/m], α, β=X,Y
$K_{d\alpha\alpha}$	$K_{\alpha\alpha}-\omega^2 M_{\alpha\alpha}$. Dynamic stiffnesses [N/m], α=X,Y
L	Bearing length [0.032 m]
M	Mass of bearing housing [kg]
M_f	Estimated mass of lubricant on housing feed plenum [kg]
$M_{\alpha\beta}$	(Estimated) Bearing fluid inertia coefficients [N.s^2/m], $\alpha=\beta$=X,Y
Re_s	$\frac{\rho\omega c^2}{\mu}$. Squeeze film Reynolds number.
T	Lubricant temperature [°C]
X,Y	Cartesian coordinate system for lateral (radial) motions of test bearing
x,y	Bearing dynamic motions along two directions X,Y [m]
WFR	$K_{xy}/C_{xx}\Omega$. Whirl frequency ratio
ε	e/c, dimensionless journal (static) eccentricity
ρ	Lubricant density [736 kg/m^3]
μ	Lubricant viscosity [Pa.s]
ω	Excitation frequency [rad/s]
Ω	Shat rotational speed [rad/s]

Introduction

High performance turbomachinery demands high shaft speeds, increased rotor flexibility, tighter clearances in the flow passages, advanced materials, and increased tolerance to imbalances. Operation at high speeds induces severe dynamic loading with large amplitude journal motions at the bearing supports. At these conditions, oil lubricated dampers and journal bearings with low levels of external pressurization are prone to air ingestion leading to an inhomogeneous lubricant film with large striations of entrapped gas. This pervasive phenomenon affects greatly the dynamic force capability of the support fluid film bearings and reduces the reliability of the rotor-bearing system.

In 2002, San Andrés [1] reported forced response experiments on a test squeeze film damper for various dynamic load conditions. Shakers exert single frequency loads and induce circular orbits and elliptical orbits of increasing amplitudes. Measurements of the applied loads, bearing displacements and accelerations allow identification of damping and inertia force coefficients for operation at three whirl frequencies (40, 50 and 60 Hz) and increasing lubricant temperatures. Measurements of film pressures reveal an early onset of air ingestion.

Identified damping force coefficients agree well with predictions based on a well-known bearing model if an effective length is used. This length ranges from 82% to 78% of the actual length as the whirl excitation frequency increases. Justifications for the reduced length or effective viscosity follow from the small through flow rate, not large enough to offset the dynamic volume changes. One damper end is flooded while the other end is open to ambient. This operating configuration thus causes pervasive air ingestion and also affects the added fluid inertia of the test bearing. Fortunately, the air entrainment models developed in past years allow quick calibration for ready prediction of the measured response, with good results for small amplitude motions.

The measurements and analysis thus show the pervasiveness of air entrainment, whose effect increases with the amplitude and frequency of the dynamic journal motions. Identified inertia coefficients are at least two times larger than predictions.

Further experiments are hereby reported to assess the effect of feed pressure and shaft speed in dynamically loaded hydrodynamic bearings. The analysis presents identified stiffness and damping force coefficients for three rotor speeds and three feed pressures.

The excitation forces are of single frequency and the resulting bearing motions are of large magnitude relative to the size of the bearing clearance. Thus, predictions based on linearized journal bearing force coefficients are expected to provide conservative estimates for the actual force coefficients derived from the test measurements.

Test rig description

Figure 1 shows a picture of the test rig and a schematic view of the rig major components and disposition. A stiff shaft[1], mounted on three precision ball bearings, holds a steel journal of diameter *(D)* 127 mm (5") and length *(L)* 32 mm (1.25"). The bearing housing comprises an acrylic bearing sandwiched by two steel circular plates. The design fluid film bearing radial clearance (c) is 0.127 mm (5 mils). The top plate (cover) includes a connection for lubricant supply through a flexible hose, a static feed pressure gauge, and four eddy current sensors facing the shaft end.

Four steel rods support the baring housing and provide a relatively soft structural stiffness to the test bearing section. Figure 2 depicts the sensor disposition and reference inertial coordinate system *(X, Y)*. Two small electromagnetic shakers hang from separate metal structures. Slender steel stingers connect the shaker heads to the bearing housing (x and y directions). Piezoelectric load cells (compression mode) at the ends of the stingers are fastened to side blocks on the bearing housing. These blocks also house two piezoelectric accelerometers *(x,y)*. The bearing housing also contains two type-K thermocouples for measurement of film temperature and two strain-gauge pressure transducers for measurement of the absolute film pressure. See prior TRC report [1] for a list of the sensors' sensitivities and ranges.

The lubrication system includes a sump tank (150 liter) and a frequency controlled main pump for supply of lubricant to the test bearing section and ball bearings supporting the shaft. An electric heater and thermostat control are located at the discharge of the main pump with a recirculation line. A flexible hose delivers the lubricant to the top of the bearing test section. Secondary pumps evacuate (suction) lubricant after discharge from the test section and ball bearings, and return the lubricant to the sump.

[1] The natural frequency of the shaft and journal is ~ 400 Hz, well above the operating speed (maximum 6,000 rpm) and excitation frequencies (0-100 Hz).

The lubricant in the experiments is an ISO VG 2 oil whose density (ρ) is 736 kg/m^3 and its viscosity (centipoise) follows the relationship $\mu(T)$=3.03 cP $e^{-0.209\,(T-23.6)}$, where T is the temperature (°C). The lubricant properties were measured in the laboratory.

Table 1 reproduces the bearing structure "dry" parameters, i.e. without lubricant flowing through the bearing. The natural frequency (f_n) of the bearing-support rods structure in the (x,y)directions is approximately 49-50 Hz. Structural cross-coupling effects are minimal. The equivalent masses noted are derived from the natural frequency measurement and also include an estimation of the mass of lubricant in the feed plenum.

Table 1. Physical parameters of bearing test section for dry (no lubricant) conditions. Reference [1]

		SI Units		English	Units
	Symbol	x-direction	y-direction	x-direction	y-direction
Structural stiffness	$(K_s)_{x,y}$	832.3 kN/m	844.2 kN/m	4756 lb/in	4824 lb/in
Equivalent mass	$(M)_{x,y}$	8.43+0.35 kg	8.55+0.35 kg	19.35 lb	19.62 lb
Damping coefficient	$(C_s)_{x,y}$	196 Ns/m	183 Ns/m	1.1 lb.s/in	1.0 lb.s/in
Damping ratio	$(\zeta)_{x,y}$	0.037	0.034		

Uncertainty in stiffness measurement 12 kN/m

Experimental procedure

Experiments for identification of journal bearing parameters are conducted with single-frequency (periodic) loads to maximize the force output from the shakers. While the shaft spins at a specified rotational speed (Ω), the shakers exert (X, Y) forces on the bearing and with frequency (ω). The external forces are expressed in general form as:

$$F_x(t)=F_{xc}\cos(\omega t)+F_{xs}\sin(\omega t)=\left(F_{xc}-iF_{xs}\right)e^{i\omega t}=\overline{F}_x e^{i\omega t}$$

$$F_y(t)=F_{yc}\cos(\omega t)+F_{ys}\sin(\omega t)=\left(F_{yc}-iF_{ys}\right)e^{i\omega t}=\overline{F}_y e^{i\omega t} \quad (1)$$

A data acquisition board and PC software collect measurements of (x, y) loads, bearing displacements and accelerations, and two film pressures. Data are recorded as ASCII files for later processing using a MATHCAD® identification software. In the data acquisition, the sampling rate is 1500 Hz with a total of 2048 recorded points. Thus, the total record time for each experiment is 1.365 s, sufficiently long to contain (at least) 20, 41 and 61 full periods of motion for excitations at 15, 30 and 45 Hz, respectively.

Table 2 presents a summary of the test conditions, namely three feed (supply) pressures, three shaft rotational speeds, and three excitation frequencies. The temperature in the film (mid plane of test bearing section) was maintained at ~ 46 ° C (115 °F) in all tests (lubricant viscosity equals 1.89 cPoise).

Table 2. Summary of test conditions and (hot) bearing (radial) clearances

Rotor speed rpm (Hz)	Excitation frequency (Hz)	Feed pressure (psig)	Clearance-x (μm)	Clearance-y (μm)
900 (15)	15, 30, 45	1, 3, 6	111.5	117.5
1,800 (30)	"	"	111.5	117.5
2,700 (45)	"	"	112.5	122.5

Bearing diametrical clearances measured immediately after each test. Nominal value $2C$=0.254 mm.

Uncertainty in measurements: pressure (0.5 psig), clearance (6 microns, ¼ mil)

Table 2 includes the magnitudes of the measured bearing radial clearances just after completing an experiment. The (hot) lubricant flows through the test section until a steady-state thermal condition is attained within the bearing. The test radial clearances are smaller than the design value (0.127 mm) and significantly different in both directions (X and Y). The hot lubricant and warm housing and shaft cause the journal expansion, thus determining a net reduction in clearance. Note that the bearing clearance in the Y-direction is (consistently) ~ 10% larger than in the X-direction. The difference needs be accounted for in the appropriate prediction of hydrodynamic fluid film forces.

The experiments aim to identify force coefficients for large orbital motions about the bearing center. The ideal null static eccentricity (ε=0) of the bearing center with respect to the journal center could not be maintained in the experiments, however. In the experiments, the static eccentricity ranged from 10% to 13% of the film clearance.

Smallest and largest eccentricity (ε) values are 4% and 15%, respectively. Nonetheless, the analysis does account for these variations in the static position.

Method for identification of bearing force coefficients

The identification procedure follows an established method for estimation of system parameters from orbital journal motions induced by single frequency forcing functions [2]. The equations of motion for the test bearing section are

$$\begin{bmatrix} M_{xx} & 0 \\ 0 & M_{yy} \end{bmatrix}\begin{Bmatrix} \ddot{x} \\ \ddot{y} \end{Bmatrix}+\begin{bmatrix} K_{xx} & 0 \\ 0 & K_{yy} \end{bmatrix}\begin{Bmatrix} x \\ y \end{Bmatrix}+\begin{bmatrix} C_{xx} & 0 \\ 0 & C_{yy} \end{bmatrix}\begin{Bmatrix} \dot{x} \\ \dot{y} \end{Bmatrix}=\begin{Bmatrix} F_x \\ F_y \end{Bmatrix}-\begin{Bmatrix} F_x \\ F_y \end{Bmatrix}_{Bearing} \tag{2}$$

where the left hand side represents the physical parameters from the bearing structural support. The bearing reaction forces are defined by the linearized description

$$\begin{Bmatrix} F_x \\ F_y \end{Bmatrix}_{Bearing} =\begin{bmatrix} C_{xx} & C_{xy} \\ C_{yx} & C_{yy} \end{bmatrix}\begin{Bmatrix} \dot{x} \\ \dot{y} \end{Bmatrix}+\begin{bmatrix} K_{xx} & K_{xy} \\ K_{yx} & K_{yy} \end{bmatrix}\begin{Bmatrix} x \\ y \end{Bmatrix} \tag{3}$$

in terms of damping $\{C_{\alpha\beta}\}_{\alpha\beta=x,y}$ and stiffness $\{K_{\alpha\beta}\}_{\alpha\beta=x,y}$ force coefficients. No added mass inertia coefficients are accounted for in the fluid film bearings. Fluid inertia effects would become apparent from the identified stiffness since this parameter actually represents $K_{\alpha\beta}-\omega^2 M_{\alpha\beta}$.

For periodic force excitations, as defined in equation (1), the bearing motions are also periodic with identical frequency (ω). Thus, the bearing displacements and accelerations are written as

$$\begin{Bmatrix} x \\ y \end{Bmatrix}=\begin{Bmatrix} x_c - i\,x_s \\ y_c - i\,y_s \end{Bmatrix}e^{i\omega t} =\begin{Bmatrix} \bar{x} \\ \bar{y} \end{Bmatrix}e^{i\omega t}\;;\;\begin{Bmatrix} \ddot{x} \\ \ddot{y} \end{Bmatrix}=\begin{Bmatrix} \bar{a}_x \\ \bar{a}_y \end{Bmatrix}e^{i\omega t} \tag{4}$$

In actuality, the bearing motions *(x, y)* include a "spurious" component due to the shaft rotation, namely the run-out motion with a fundamental frequency coinciding with

the shaft speed (Ω). In the analysis of the acquired displacements and accelerations, a Fourier series decomposition of the time series establishes that

$$x(t)=x_o+\bar{x}\,e^{i\omega t}+\bar{x}_B\,e^{i\Omega t};\; y(t)=y_o+\bar{y}\,e^{i\omega t}+\bar{y}_B\,e^{i\Omega t} \tag{5}$$

where (x_o, y_o) denote the static offset (eccentricity) and $(\bar{x}_B, \bar{y}_B)$ represent the baseline motion components from the shaft rotation. In the physical operation of the test rotor, these last motions appear even without external forced excitation. Figure 3 shows a typical bearing motion recorded at a rotor speed of 1,800 rpm (30 Hz) and due to a forced excitation with a frequency of 15 Hz. The graph also includes the curve fits, from Fourier analysis, showing (a) only the excitation frequency component, and (b) the Fourier components due to the excitation frequency (ω) and rotor sped (1X). The bottom graph depicts the FFT of the displacement showing two fundamental frequencies, namely the forced excitation (15 Hz) and the one synchronous with rotor speed (30 Hz=1X).

With the definitions introduced, the equations of motion reduce to

$$\begin{bmatrix} H_{xx} & H_{xy} \\ H_{yx} & H_{yy} \end{bmatrix} \begin{Bmatrix} \bar{x} \\ \bar{y} \end{Bmatrix} = \begin{Bmatrix} \bar{F}_{xB} \\ \bar{F}_{yB} \end{Bmatrix} = \begin{Bmatrix} \bar{F}_x - M_{xx}\,\bar{a}_x - (K_{xx}+i\omega C_{xx})\bar{x} \\ \bar{F}_y - M_{xy}\,\bar{a}_y - (K_{xy}+i\omega C_{xy})\bar{y} \end{Bmatrix} \tag{6a}$$

or

$$\mathbf{H}_B\,\mathbf{z}_B = \mathbf{f}_B \tag{6b}$$

where $\mathbf{H_B}$ represents the matrix of bearing impedances, i.e. $\left(H_{\alpha\beta}=K_{\alpha\beta}+i\omega C_{\alpha\beta}\right)_{\alpha\beta=x,y}$, $\mathbf{z}_B=[\bar{x}\quad \bar{y}]^T$, and $\mathbf{f}_B=[\bar{F}_{xB}\quad \bar{F}_{yB}]^T$. Equations (6) represent two algebraic equations (x,y) and the number of (complex) bearing parameters to be determined is four. Two external forcing functions, $\mathbf{f_1}$ and $\mathbf{f_2}$, will produce two bearing reaction forces, $\mathbf{f_{B1}}$ and $\mathbf{f_{B2}}$, and two displacement vectors, $\mathbf{z_{B1}}$ and $\mathbf{z_{B2}}$, respectively. The two excitation periodic force vectors, $\mathbf{f_1}$ and $\mathbf{f_2}$, of identical frequency (ω) must be linearly independent. In particular, forces rendering circular bearing orbits are not desirable.

Hence, the equations for the bearing impedances become

$$\mathbf{H}_B [\mathbf{z}_{B1} \quad \mathbf{z}_{B2}] = [\mathbf{f}_{B1} \quad \mathbf{f}_{B2}] \tag{7}$$

, and the bearing coefficients are determined from solution of

$$\mathbf{H}_B = \begin{bmatrix} K_{xx} + i\omega C_{xx} & K_{xy} + i\omega C_{xy} \\ K_{yx} + i\omega C_{yx} & K_{yy} + i\omega C_{yy} \end{bmatrix} = [\mathbf{f}_{B1} \quad \mathbf{f}_{B2}] \, [\mathbf{z}_{B1} \quad \mathbf{z}_{B2}]^{-1} \tag{8}$$

A MATHCAD worksheet processes the recorded time data series (forces, displacements and accelerations); determines the Fourier coefficients (excitation frequency, (ω); and synchronous with rotor speed, (Ω)); subtracts the shaft run-out displacement if $\omega=\Omega$; builds the system of equation (6) for each forced excitation; and solves equation (8) for identification of the bearing force coefficients. Graphical output is readily available; including comparisons to predictions based on the short length journal bearing model [3].

During each test, three identical sets of two independent forced excitations are exerted on the bearing and the displacements and accelerations recorded. The extracted force coefficients are an average of the three sets. Standard deviations for each bearing coefficient are also calculated.

Figure 4 depicts the baseline shaft (run out) motion, i.e. without external force excitation, for the three test speeds at a feed pressure of 1 psig (0.07 bar). The graphs include the time series constructed with the Fourier (complex) coefficient determined for the fundamental frequency, synchronous, coinciding with rotor speed. The run-out shaft amplitudes of motion are not insignificant and largest at a speed of 1,800 rpm (30 Hz), closest to the critical speed (damped natural frequency) of the system. For operation at 30 Hz, the amplitudes of synchronous shaft (run-out) motion are approximately 20 μm and 16 μm in the (x, y) directions, respectively. These amplitudes amount to 16% and 13% of the nominal film clearance (125 μm).

Figure 5 depicts the two independent excitation force sets exerted for identification of the bearing force coefficients. The forces are single frequency (ω); in a first test, the amplitude of F_x is larger than that of F_y. The converse follows for the second test, i.e. $|F_y|$

$> |F_x|$. The amplitude of the largest force is maintained at about 75 N (16.9 lb), while the other force amplitude is 50% less, i.e. ~ 38 N (8.5 lb). The graphs contain the recorded data (forces) and the single-frequency curve fit using the fundamental Fourier coefficients.

Figure 6 shows the bearing dynamic forced response to the two external force sets. The results correspond to a rotor speed of 1800 rpm (30 Hz), excitation frequency equal to 15 Hz, and at a feed pressure of 3 psig (0.2 bar). The graphs on the left correspond to a first test with $|F_x| > |F_y|$, while those on the right are for $|F_y| > |F_x|$. The top graphs show the actual bearing displacements and the (analytically determined) periodic motion at the excitation frequency (15 Hz). The bottom graphs also show the actual test data and the analysis-based motion including the superposition of the motions due to the forced excitation (15 Hz) and that synchronous with rotor speed (30Hz). Note that the Fourier analysis reproduces accurately the bearing dynamic motions.

Figure 7 reproduces in dimensionless form the bearing displacements (X vs Y) shown in Figure 6. The recorded (hot) clearance of 0.114 mm is used to render the dimensionless motions. Note that the bearing orbital amplitudes of motion exceed 60% of the bearing nominal clearance. Thus, the extracted force coefficients are not representative of the linearized force coefficients typically found in the literature [4].

Appendix A shows the test data, excitation forces and ensuing bearing orbital motions, for the tests conducted with a feed pressure equal to 3 psig. The graphs include the Fourier analysis decomposition due to the excitation force with frequency (ω) and synchronous (Ω) with rotor speed.

Experimental bearing stiffness and damping coefficients

Stiffness and damping force coefficients are estimated from the measured excitation forces and ensuing bearing orbital motions at various rotor speeds and excitation frequencies. The Figures below display the identified coefficients in graphical form. For purposes of comparison, analytical force coefficients derived from the short-length journal bearing model are also included. Note that the theoretical force coefficients are strictly valid for infinitesimally small amplitude journal motions about a static equilibrium position.

In the experiments, the bearing static position is within 15% of its center (relatively small static eccentricity). Thus, predictions show the typical symmetry for the direct force coefficients, i.e. $K_{xx} \sim K_{yy}$, $C_{xx} \sim C_{yy}$; while the cross-coupled stiffness coefficients are anti-symmetric, i.e. $K_{xy} \sim -K_{yx}$. For laminar flow journal bearings it also follows that $C_{xy} = C_{yx}$ for all eccentricities. The stiffness coefficients are proportional to rotor speed (Ω).

The tests were conducted at three increasing supply pressures. For the lowest feed pressure (~ 1 psig), lubricant cavitation may easily occur, while for the largest feed pressure (~ 6 psig), a full film over the entire flow area should evolve[2]. Thus, predicted linearized force coefficients are shown for the two conditions, namely a cavitated film (half-film or π extent) and full film (no cavitation). Lubrication theory indicates that the relationships between the force coefficients for these two extreme conditions is [5]:

$$\begin{aligned} \left(K_{xx}, K_{yy}, C_{xy}, C_{yx}\right)_{full\ film} &\approx 0 \\ \left(K_{xy}, K_{yx}, C_{xx}, C_{yy}\right)_{full\ film} &\approx 2\left(K_{xy}, K_{yx}, C_{xx}, C_{yy}\right)_{cavitated} \end{aligned} \tag{9}$$

The static eccentricities (ε) obtained from the measurements and the rotor speed define the linearized force coefficients, which are not functions of the excitation frequency. The graphs below depict predicted average values for the test conditions noted. The formula for the π-film short length bearing force coefficients are [6]:

$$\begin{pmatrix} K_{xx} & K_{xy} \\ K_{yx} & K_{yx} \end{pmatrix} = \mu(T)\cdot\frac{D}{2}\cdot\left(\frac{L}{c}\right)^3\cdot\Omega\cdot\begin{bmatrix} \dfrac{2\cdot\varepsilon\cdot\left(1+\varepsilon^2\right)}{\left(1-\varepsilon^2\right)^3} & \dfrac{\pi}{4\cdot\left(1-\varepsilon^2\right)^{1.5}} \\ \dfrac{\pi\cdot\left(1+2\cdot\varepsilon^2\right)}{4\cdot\left(1-\varepsilon^2\right)^{2.5}} & \dfrac{\varepsilon}{\left(1-\varepsilon^2\right)^2} \end{bmatrix}$$

$$\begin{pmatrix} C_{xx} & C_{xy} \\ C_{yx} & C_{yx} \end{pmatrix} = \mu(T)\cdot\frac{D}{2}\cdot\left(\frac{L}{c}\right)^3\cdot\begin{bmatrix} \dfrac{\pi\cdot\left(1+\varepsilon^2\right)}{\left(1-\varepsilon^2\right)^{2.5}\cdot 2} & \dfrac{-2\cdot\varepsilon}{\left(1-\varepsilon^2\right)^2} \\ \dfrac{-2\cdot\varepsilon}{\left(1-\varepsilon^2\right)^2} & \dfrac{\pi}{2\left(1-\varepsilon^2\right)^{\frac{3}{2}}} \end{bmatrix} \tag{10}$$

[2] The specific dynamic pressure equals to the magnitude of the dynamic load divided by the bearing projected area (L D). For a peak load magnitude of 75 N (16.9 N), the maximum specific pressure is 2.7 psi (0.2 bar).

For operation at very small eccentricities $(\varepsilon \to 0)$, it follows that $C_{xy} = C_{yx} = 0$; $K_{xx} = K_{yy} = 0$, i.e. no direct stiffness support; and ,

$$C_{xx} = C_{yy} = \frac{\pi \mu D L^3}{4c^3}; \; K_{xy} = -K_{yx} = C_{xx}\frac{\Omega}{2}; \; WFR = \frac{K_{xy}}{C_{xx}\Omega} = \frac{1}{2} \qquad (11)$$

where the whirl frequency ratio (WFR)~0.50 is the stability indicator for plain journal bearings.

Figure 8 displays the experimentally derived cross-coupled stiffness coefficients (K_{xy}, K_{yx}) versus rotor speed for the three feed pressures. The test results do not distinguish the various excitation frequencies (more on this issue later). In general, the identified coefficients show the expected asymmetry, $K_{xy} \sim -K_{yx}$. The predictions agree reasonably with the test derived coefficients and indeed bracket them, i.e. the full film and cavitated film model predictions are upper and lower bounds for the identified parameters. The standard deviation (uncertainty) follows later.

Figure 9 shows that the identified journal bearing direct damping coefficients (C_{xx}, C_{yy}) lie within the predicted coefficients for the full film and cavitated film conditions. Note that the test $C_{xx} \sim C_{yy}$, i.e. nearly identical. As expected, the damping coefficients are not strong functions of the rotor speed, although C_{yy} seems to decrease as the rotor speed increases. In general, the direct damping coefficients for the low feed pressure are smaller in magnitude than for the other larger supply pressures.

Figure 10 depicts the test cross-coupled damping coefficients (C_{xy}, C_{yx}) versus rotor speed for the three feed pressures. The predicted coefficients are null for the full film condition and identical for the cavitated film, i.e. $C_{xy} \sim C_{yx}$. However, the experimentally derived coefficients show an asymmetric behavior, i.e. $-C_{yx} = C_{xy}$, in particular at rotor speeds of 900 rpm and 1800 rpm. The test coefficients differ largely at the highest rotor speed of 2700 rpm. The asymmetric behavior is typical of fluid inertia effects, not accounted for in the predictive analysis.

Figure 11 displays the identified direct stiffness coefficients (K_{xx}, K_{yy}) versus rotor speed for the three test feed pressures. The predicted stiffness are null for the full film condition and nearly identical for the cavitated film, i.e. $K_{xx} \sim K_{yy}$. Incidentally, the

analytical direct stiffnesses are small in magnitude relative to the cross-coupled stiffnesses since the bearing eccentricity is small (< 15%). On the other hand, the test derived stiffness coefficients (K_{xx}, K_{yy}) are mostly negative and of large amplitude, in particular at low rotor speeds. The experimental coefficients do not make much sense until the effect of the excitation frequency is brought into perspective.

Note that the estimated direct coefficient (K_{xx}) in actuality represents the dynamic stiffness $K_{xxd} = K_{xx} - \omega^2 M_{xx}$, and since $K_{xx} \sim 0$, the added mass coefficient equals $M_{xx} = -K_{xxd}/\omega^2$. Thus, the excitation frequency (read fluid inertia effects) plays a major role on the performance of the test bearing. Figure 12 shows the identified direct (dynamic) stiffness coefficients (K_{xx}, K_{yy}) versus excitation frequency for the three supply pressures and three rotor speeds. Note that the direct stiffnesses are clearly frequency dependent. A quadratic curve fit to the test coefficients[3] shows that M_{xx}=11.4 kg, M_{yy}=6 kg. The predicted added mass coefficient equals $\frac{\pi \rho D L^3}{20c}$ = 3.79 kg [5], i.e. a fraction of the test derived parameter. Note that the squeeze film Reynolds number ($Re_s = \rho \omega c^2/\mu$) at the largest frequency (45 Hz) is just 1.78.

The large difference between the predicted added mass coefficient and the derived inertia coefficients cannot be easily explained. However, prior experiments with the same test rig [1] operating in a squeeze film damper mode show a direct inertia coefficient ~ 6.5 kg for forced excitations at 40 Hz. As noted in [1], the discrepancy is typical and probably due to the type of end conditions in the test bearing, namely one end open to a flooded (feed) plenum and the other open to ambient (discharge).

Table 3 provides the largest standard deviations derived from three identical experiments. For each supply pressure, the shaft speed (900 rpm) and excitation frequency are noted. The lowest standard deviations, on the order of a few percent, correspond to the cross-coupled stiffnesses and the direct damping coefficients. On the other hand, the standard deviations for the direct stiffnesses are as large as 23% The cross-coupled damping coefficients show the worst deviations. Note that 900-rpm shaft speed tests consistently render the largest standard deviations.

[3] The curve fit includes the data for the three rotor speeds (900, 1800 and 2700 rpm) and the three supply pressures (1, 3 and 6 psig).

Table 3. Largest standard deviations for identified force coefficients at three feed pressures

	pressure psig	speed RPM	freq Hz	KXX N/m	KXY	KYX	KYY	CXX Ns/m	CXY	CYX	CYY
Mean value	1	900	45	-8.68E+05	2.37E+05	-1.44E+05	-4.57E+05	6457	466	-551	5017
	3	900	30	-2.76E+05	3.61E+05	-1.68E+05	-2.84E+05	7194	-122	-994	6116
	6	900	30	-3.00E+05	4.47E+05	-3.93E+05	-3.06E+05	8038	-77	-1240	6319
Maximum Standard Deviation											
	pressure	speed	freq	KXX	KXY	KYX	KYY	CXX	CXY	CYX	CYY
	1	900	45	3.84E+04	2.80E+04	3.83E+04	1.72E+04	79	143	143	111
	3	900	30	4.61E+04	2.04E+04	3.45E+04	2.99E+04	177	267	267	161
	6	900	30	6.98E+04	1.98E+04	2.39E+04	5.83E+04	349	350	350	146
Percent deviation from mean value parameter											
	pressure	speed	freq	KXX	KXY	KYX	KYY	CXX	CXY	CYX	CYY
	1	900	45	4	12	27	4	1	31	26	2
	3	900	30	17	6	20	11	2	219	27	3
	6	900	30	23	4	6	19	4	453	28	2

Figure 13 depicts the whirl frequency ratio (*WFR)* for the test bearing, as derived from the experimentally identified force coefficients. The *WFR* approaches 0.5 at the largest rotor speed, agreeing with the analytical predictions. The *WFR*~0.40 at the lowest rotor speed is typical. Feed pressure and excitation frequency do not have a significant effect of the bearing stability parameter.

Conclusions

Experiments were conducted to assess the dynamic response of a plain journal bearing undergoing large orbital motions due to single-frequency excitation forces. The short test bearing of slenderness ratio L/D=0.25 has a nominal radial clearance equal to 0.127 mm (5 mils). Tests were conducted at three rotor speeds (900, 1800 and 2700 rpm), three feed pressures (1, 3 and 6 psig), and three excitation frequencies (15, 30 and 45 Hz).

A pair of electromagnetic shakers excites the bearing structure along two orthogonal directions while the shaft spins at a selected speed. A DAQ system records the bearing motions and accelerations and the exerted dynamic forces. The Fourier analysis of the test data extracts the components of forces and bearing motions due to the excitation frequency and proceeds to identify the bearing force coefficients, stiffness and damping, using an established procedure. Baseline bearing motions due to shaft run-out are recorded and subtracted in the parameter identification procedure. The forces exerted on the bearing induce large orbital motions with peak amplitudes exceeding 50% of the

nominal bearing clearance. Thus, the extracted force coefficients do not represent the typical linearized (rotordynamic) force coefficients.

The experimentally identified force coefficients are compared with force coefficient predictions based on the short length bearing model for conditions of full film and π-film cavitation. The analytical direct damping coefficients and cross-coupled stiffness coefficients agree favorably with the experimental coefficients, thus demonstrating that linearized force coefficients, strictly valid for small amplitude motions, do fairly well in predicting bearing motions of large amplitude. The experimental whirl frequency ratio, a well-known stability parameter for bearing dynamic performance, shows the typical 50% value at the highest speed tested. The test cross-coupled damping coefficients do not agree well with the theoretical predictions; however, their impact on the forced response appears to be not significant. On the other hand, the excitation frequency has a marked influence of the test direct stiffness coefficients; hence evidencing large fluid inertia effects even though the operating conditions show a squeeze film Reynolds number of order one. Test derived direct inertia force coefficients are (at least) twice larger than the analytical values.

Further experiments and analysis will continue in the following months. Tests with the bearing off-centered to 25, 50 and 75 % of the clearance are currently being conducted.

References

[1] San Andrés, L., 2002, "Response of a Squeeze Film Damper Under High Dynamic Loading and Identification of Damping and Inertia Coefficients," TRC-SFD-1-02.

[2] Diaz, S. and L. San Andrés, L., 2000, "Orbit-Based Identification of Damping Coefficients on Off-Centered Squeeze Film Dampers Including Support Flexibility," ASME Paper 2000-GT-0394.

[3] San Andrés, 2003, MATHCAD program for identification of hydrodynamic journal bearing force coefficients, Turbomachinery Laboratory, proprietary software, March.

[4] Childs, D., 1993, "Tubromachinery Rotordynamics," John Wiley Interscience Pubs.

[5] San Andrés, L., 2000, "Modern Lubrication Theory," Graduate Class Course Notes, Texas A&M University, Mechanical Engineering Department.

[6] Vance, J., 1988, "Rotordynamics of Turbomachinery," John Wiley Interscience Pubs.

Colophon

The undergraduate students also conducted a number of experiments with the test bearing operating in a squeeze film damper (SFD) mode for centered and (large) off-centered static positions. The tests aim to determine quantitatively the effect of increasing supply pressures on damper force coefficients and to extract SFD force coefficients from multiple-frequency excitation forces (sine-sweep). The Principal Investigator developed identification programs for chirp-forced functions and will perform the analysis of the experimental data in the summer of 2003.

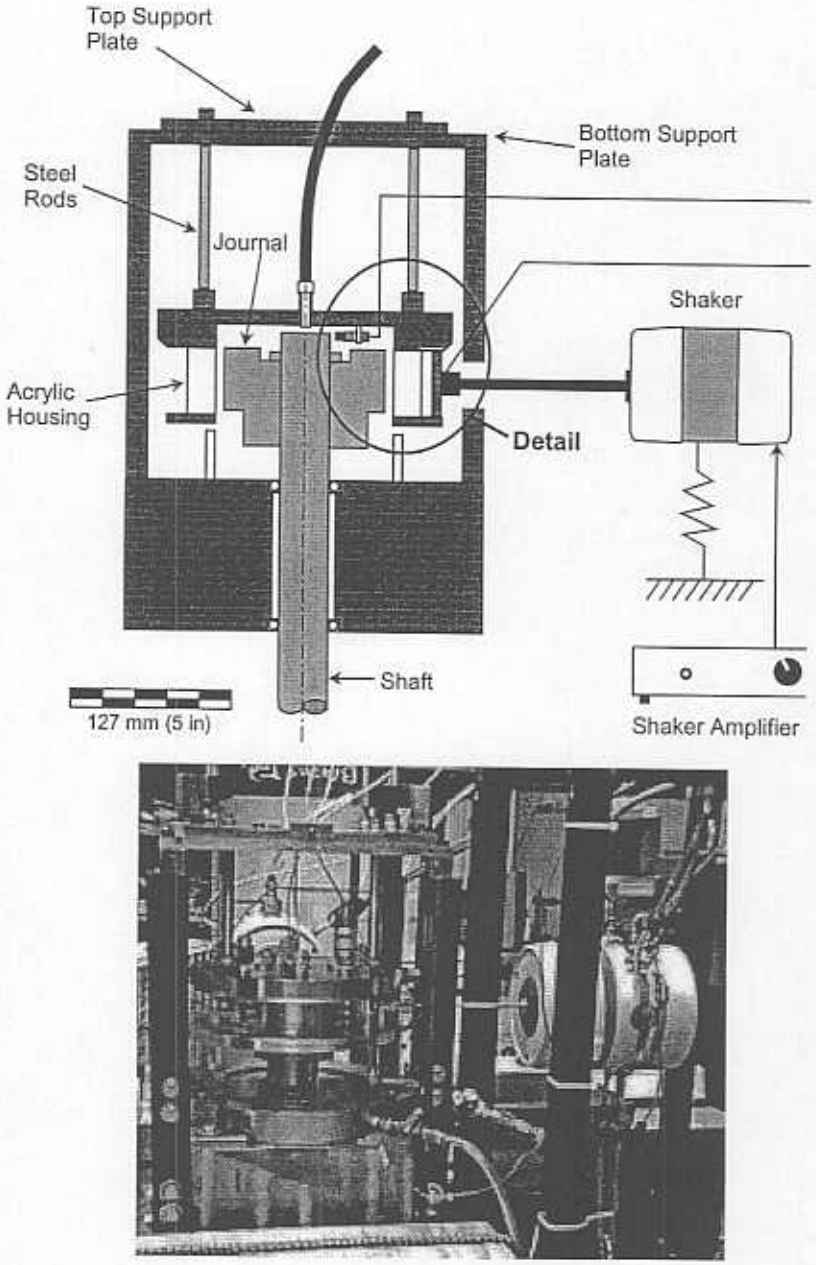

Figure 1 Test rig for identification of fluid film bearing force coefficients

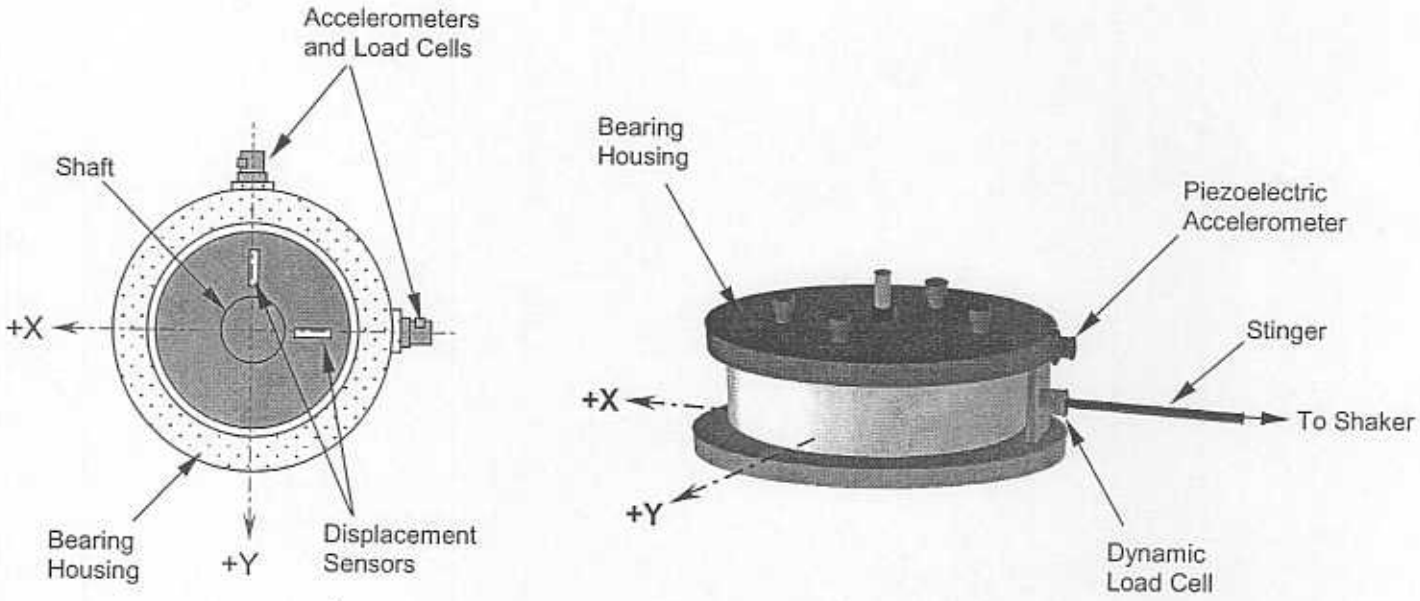

Figure 2. Positions of sensors and reference coordinate system

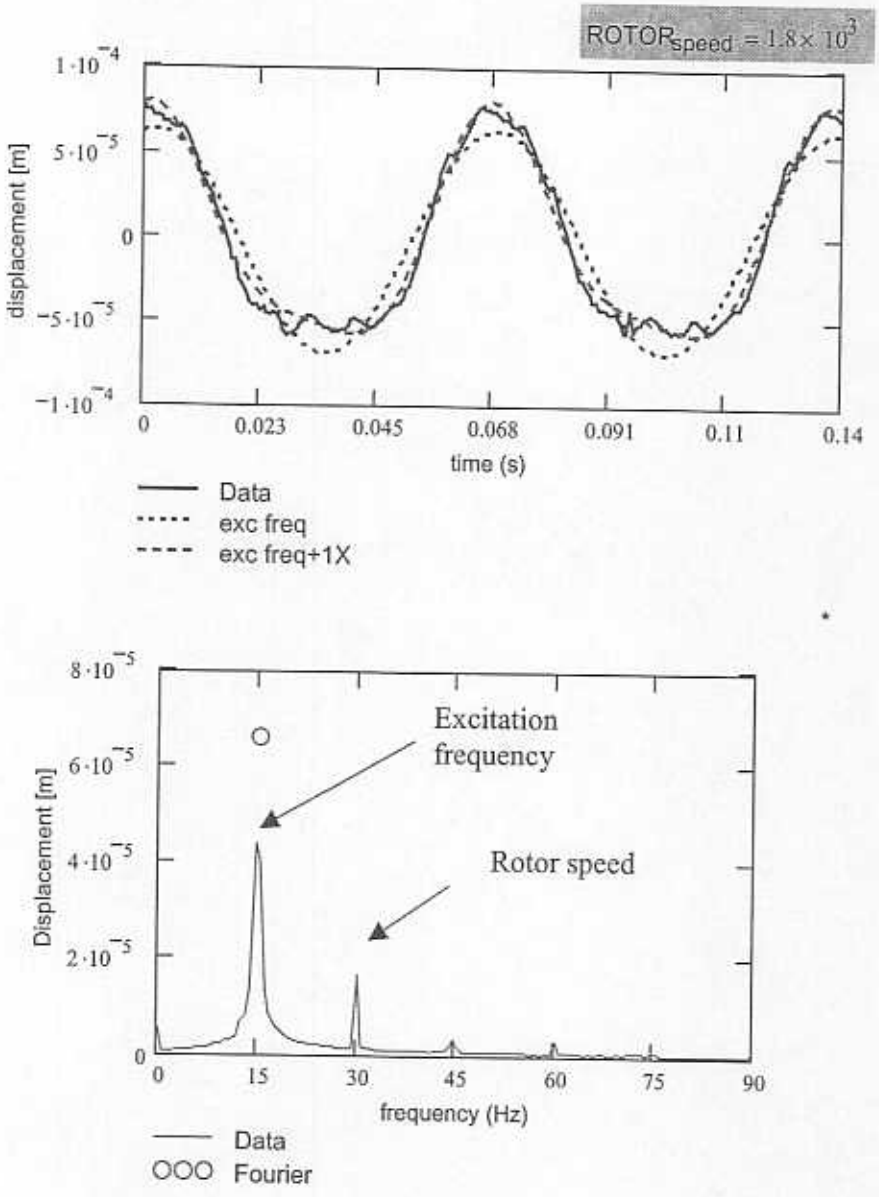

Figure 3 Typical bearing motion (x) for forced excitation at frequency (15 Hz) and rotor speed of 1,800 rpm (30 Hz). Data and curve fits (Fourier coefficients) including excitation frequency and rotor speed. Top: Time series, Bottom: FFT of displacement and Fourier coefficients

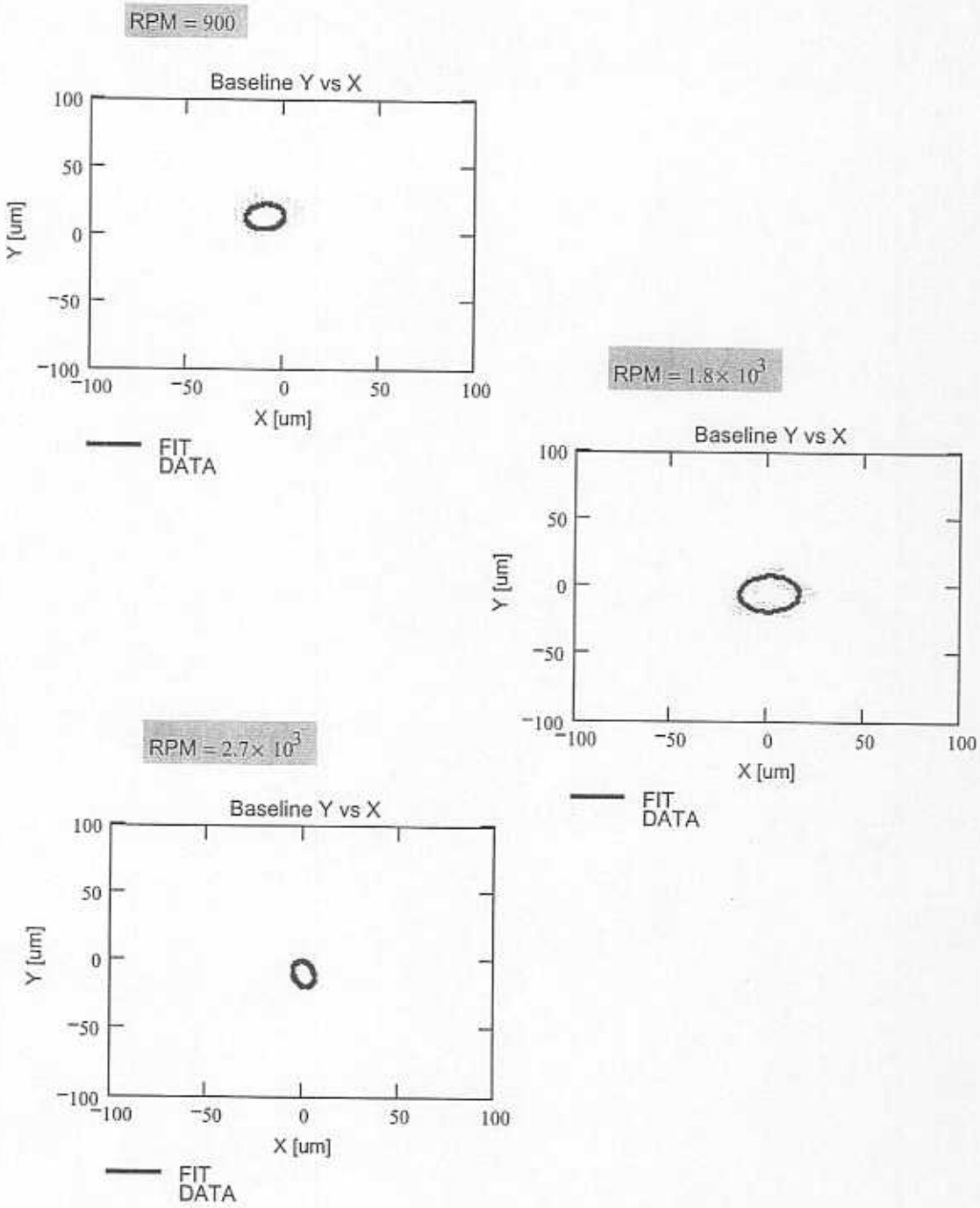

Figure 4 Baseline (run out) shaft motion (no forced excitation) at rotor speeds of 900 rpm, 1,800 rpm, and 2,700 rpm. Feed pressure = 1 psig. Data and curve fit with fundamental rotor speed (1X)

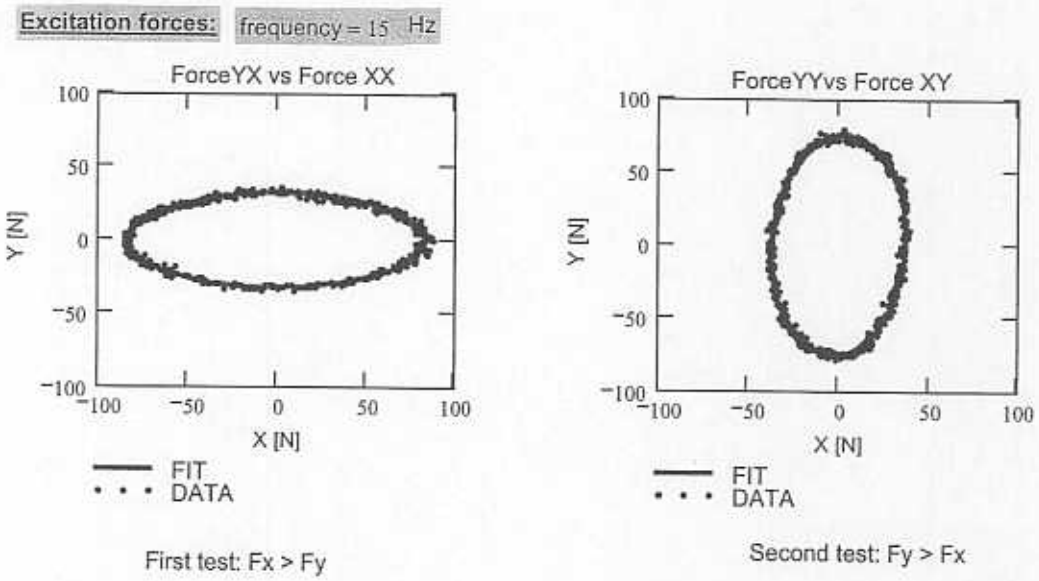

Figure 5 Independent, single-frequency, excitation force sets (F_x, F_y) exerted on fluid film bearing. Left: $|F_x| > |F_y|$, Right: $|F_y| > |F_x|$. Data and curve fit with fundamental frequency (ω=15 Hz)

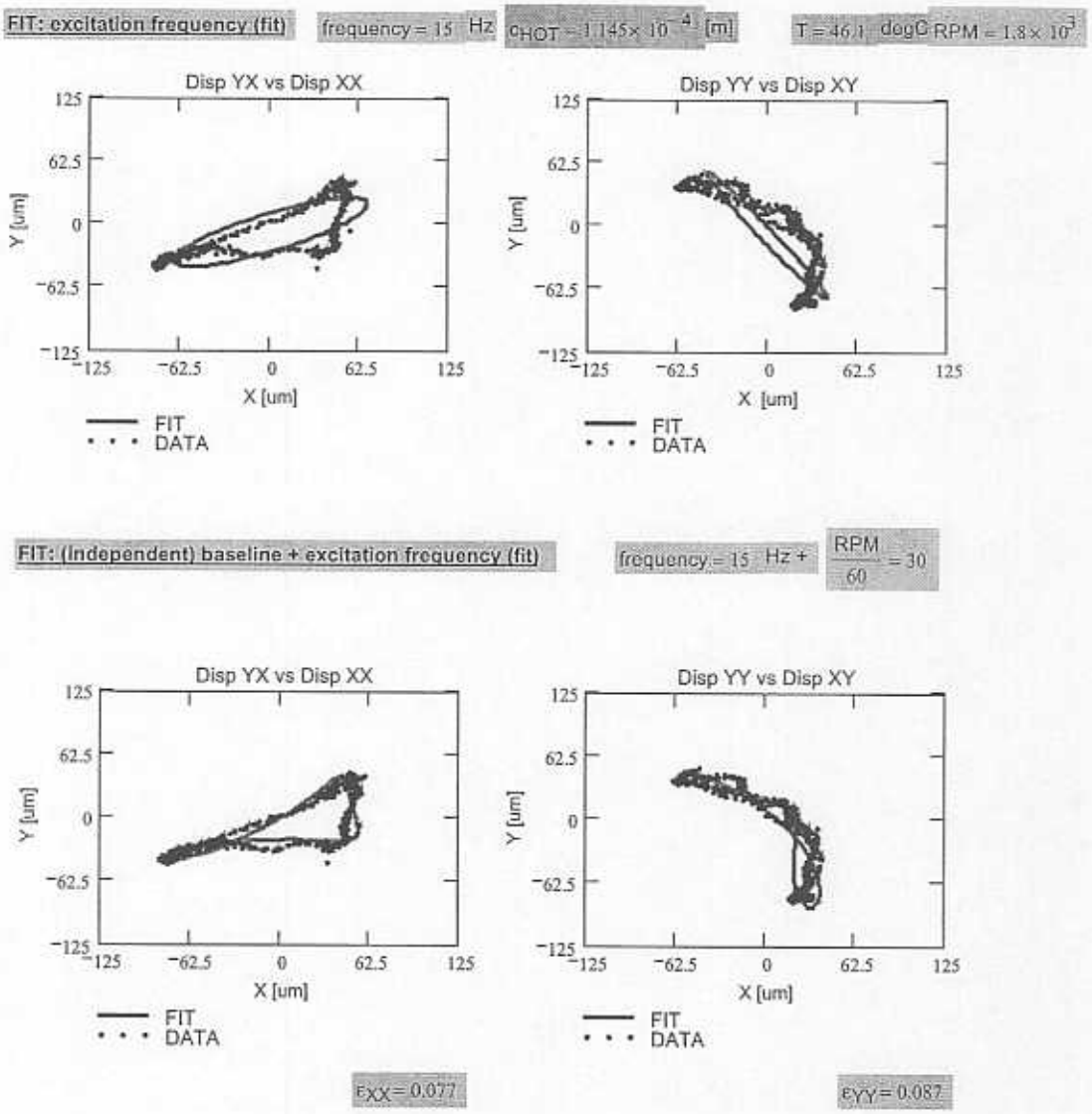

Figure 6. Bearing dynamic response for test at shaft speed 1800 rpm (30 Hz) and excitation frequency (15 Hz), feed pressure 3 psig. Left: $|F_x| > |F_y|$, Right: $|F_y| > |F_x|$, Top: Bearing motions (X,Y) in μm, data and excitation frequency component; Bottom: Bearing motions (X,Y) in μm, data and excitation plus synchronous shaft speed components

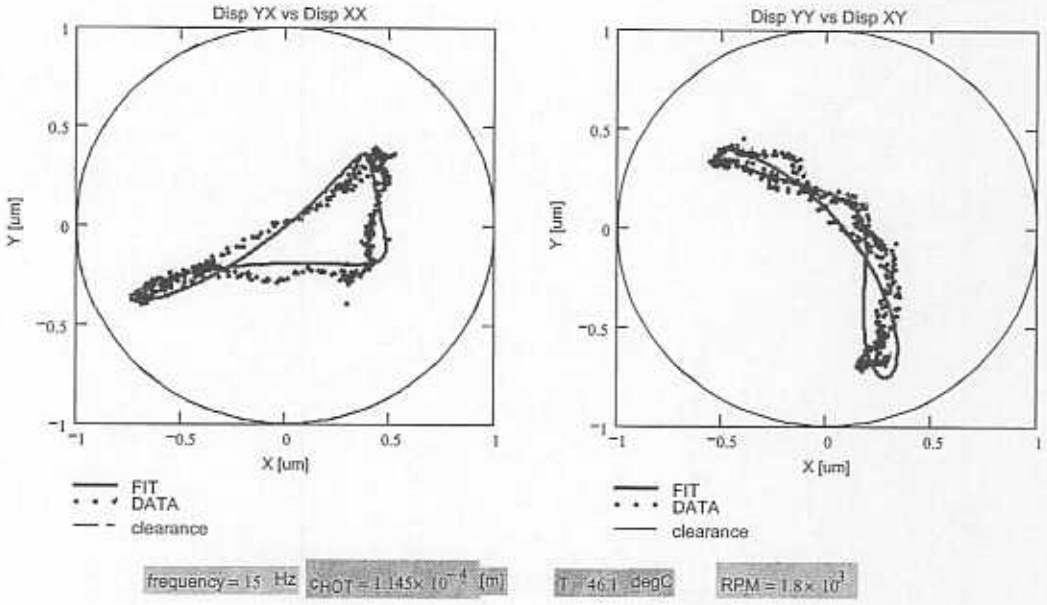

Figure 7 Dimensionless (*X*,*Y*) bearing displacements for test at shaft speed 1800 rpm (30 Hz) and excitation frequency (15 Hz), feed pressure 3 psig. Left: $|F_x| > |F_y|$, Right: $|F_y| > |F_x|$

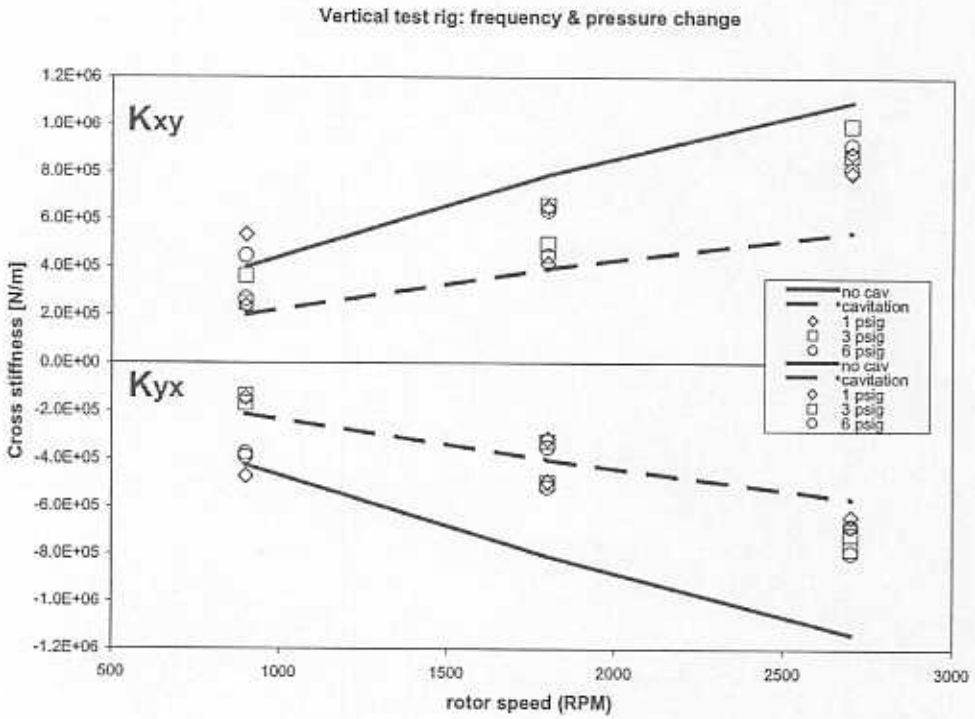

Figure 8 Estimated and predicted cross-coupled stiffness coefficients (K_{xy}, K_{yx}) vs rotor speed. Test data for three feed pressures and excitation frequencies (15, 30, 45 Hz). Analytical coefficients for full film and π-film (cavitated) conditions

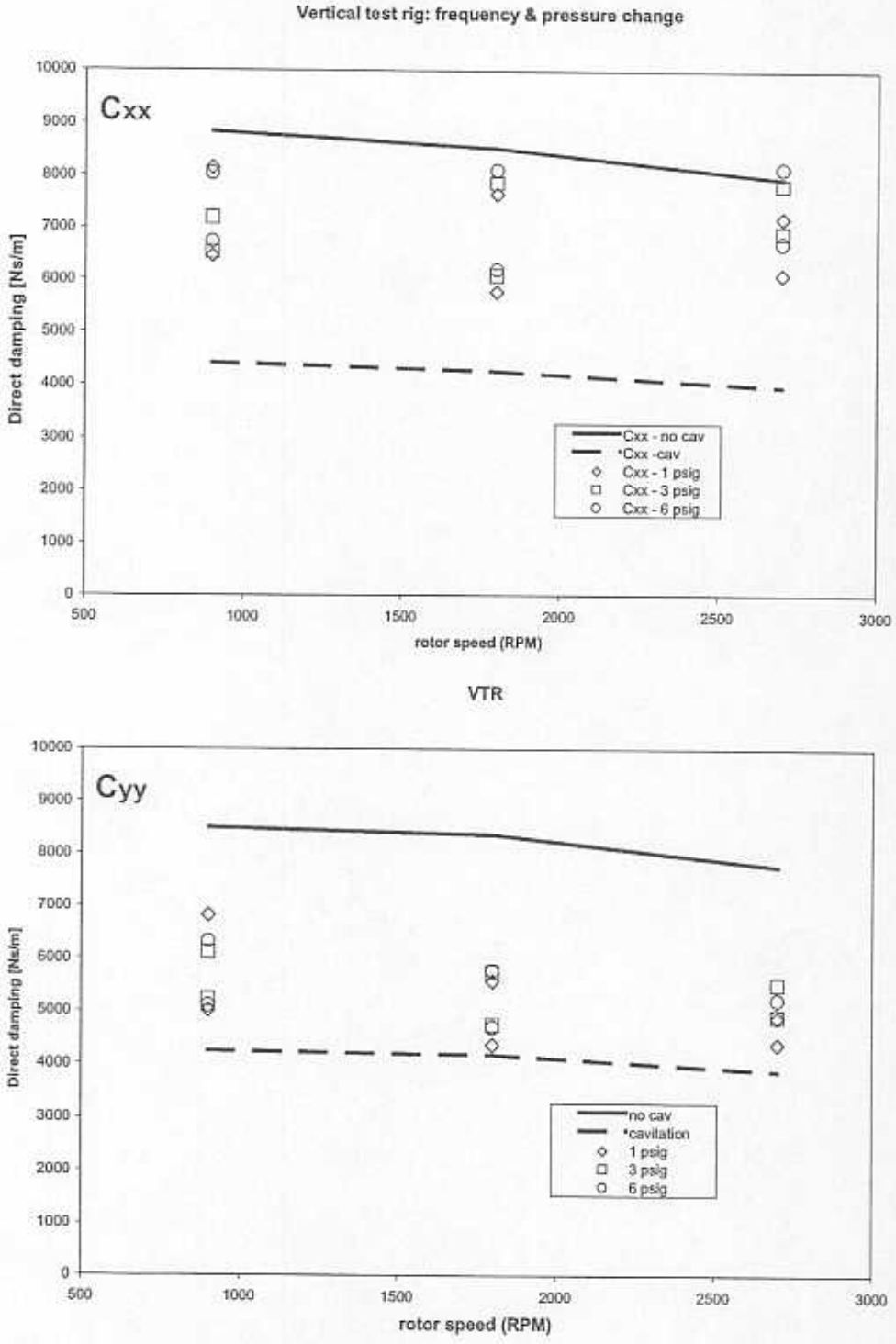

Figure 9 Estimated and predicted direct damping coefficients (C_{xx}, C_{yy}) vs rotor speed. Test data for three feed pressures and excitation frequencies (15, 30, 45 Hz). Analytical coefficients for full film and π-film (cavitated) conditions

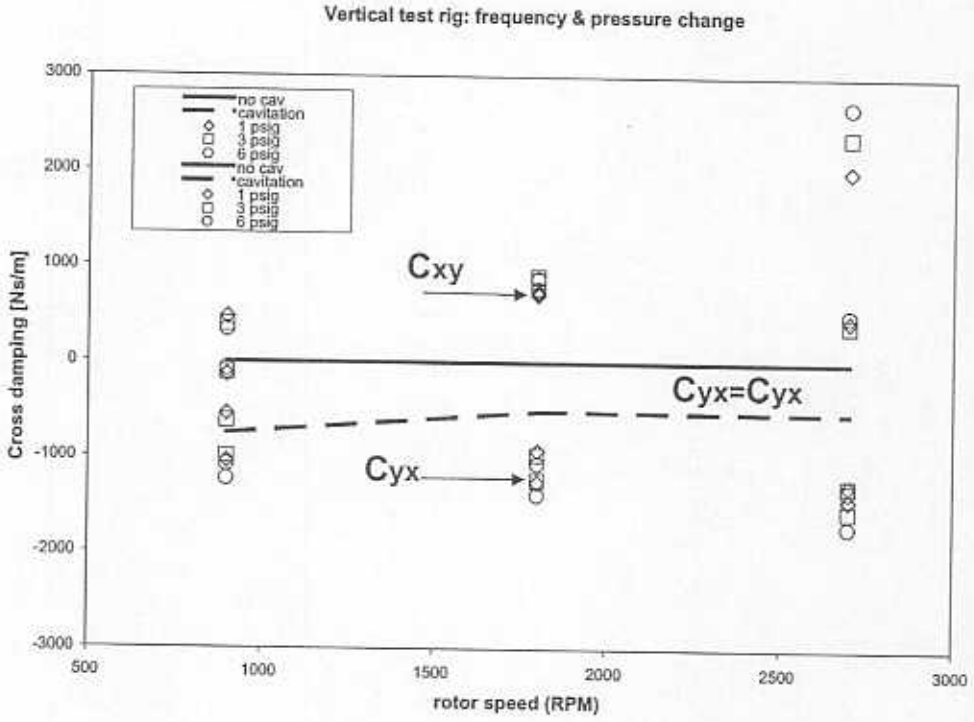

Figure 10 Estimated and predicted cross-coupled damping coefficients (C_{xy}, C_{yx}) vs rotor speed. Test data for three feed pressures and excitation frequencies (15, 30, 45 Hz). Analytical coefficients for full film and π-film (cavitated) conditions

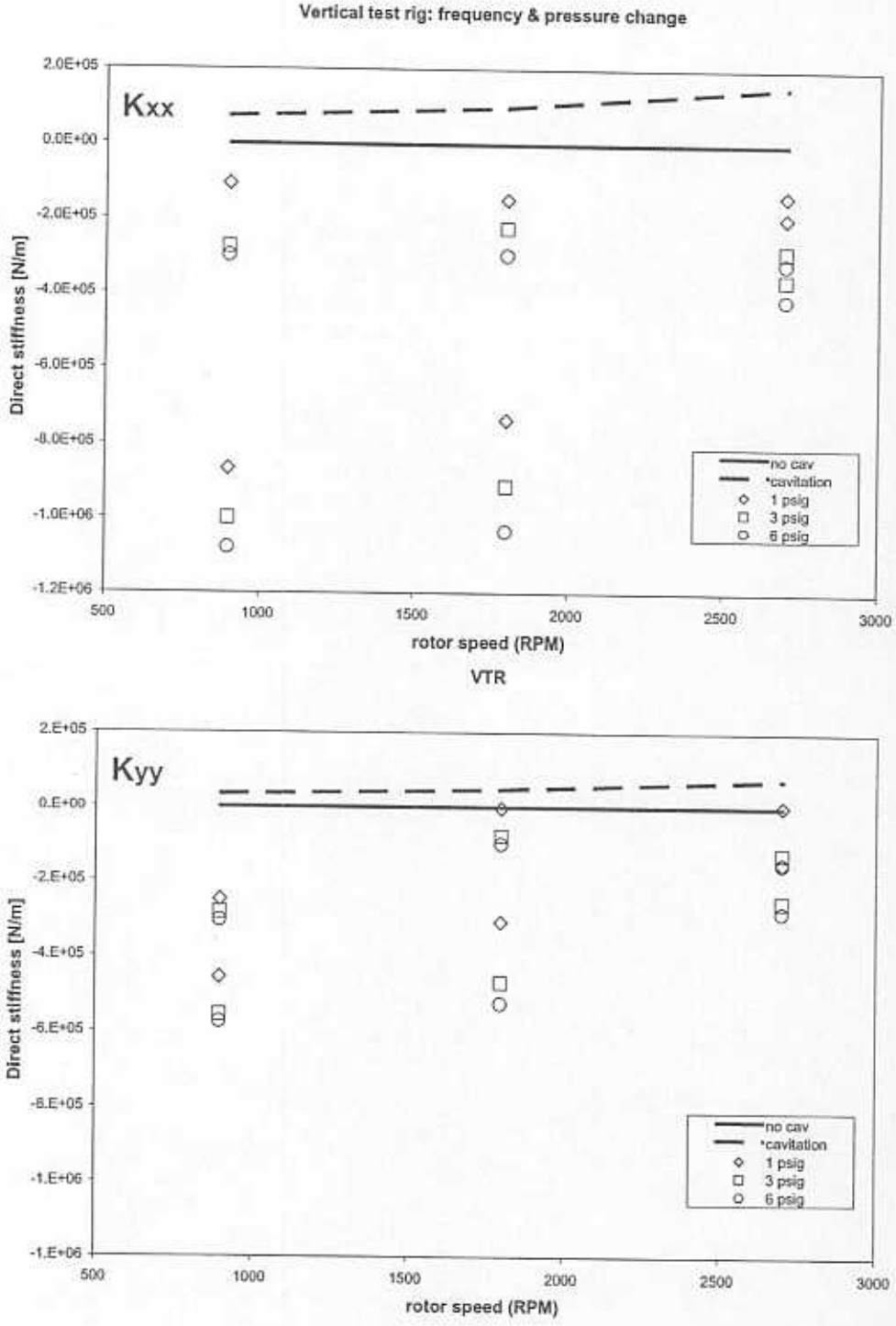

Figure 11 Estimated and predicted direct stiffness coefficients (K_{xx}, K_{yy}) vs rotor speed. Test data for three feed pressures and excitation frequencies (15, 30, 45 Hz). Analytical coefficients for full film and π-film (cavitated) conditions

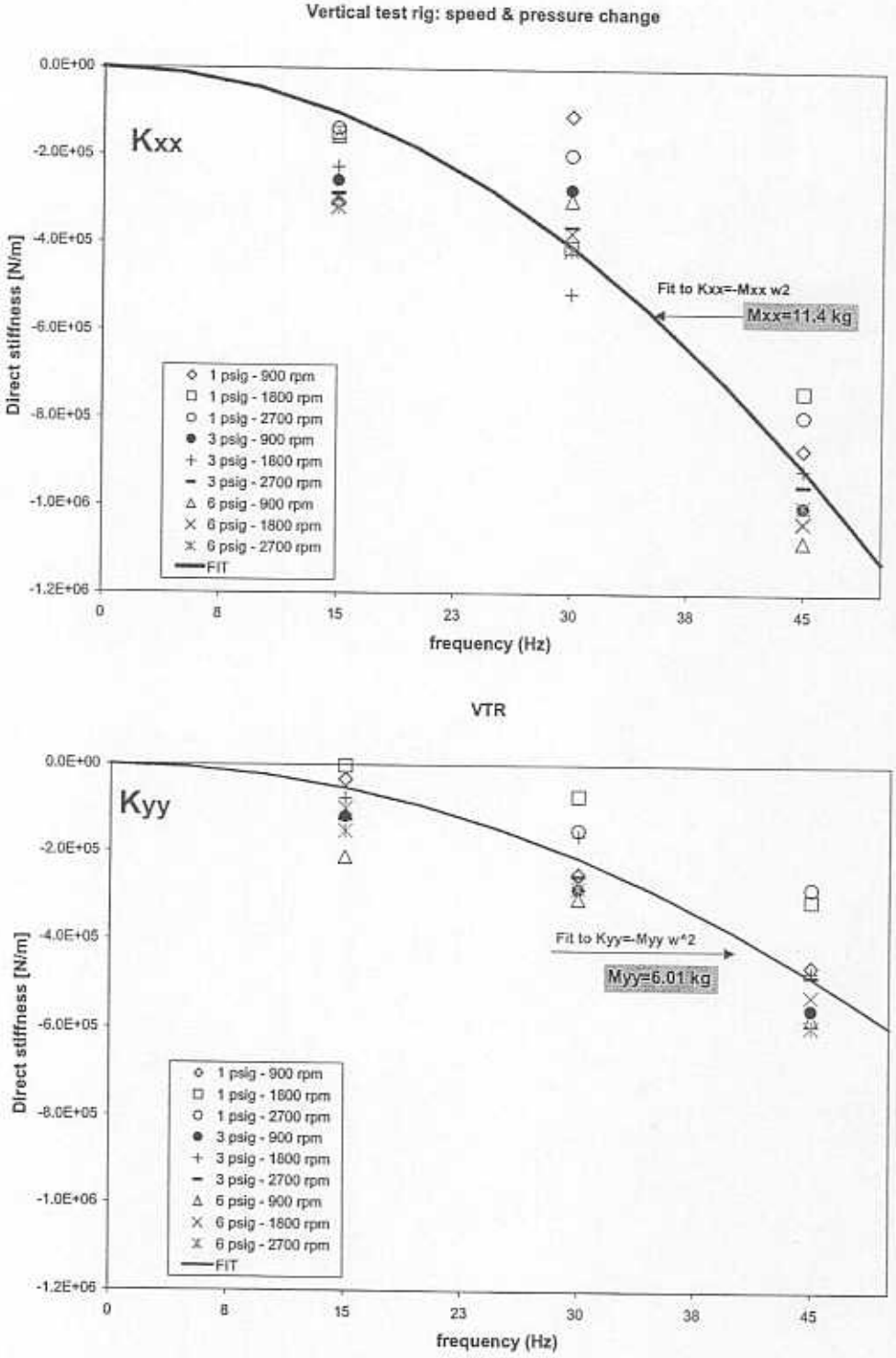

Figure 12 Estimated direct stiffness coefficients (K_{xx}, K_{yy}) vs excitation frequency. Data for three feed pressures and rotor speeds (15, 30, 45 Hz). Quadratic curve showing inertia coefficients (M_{xx}, M_{yy})

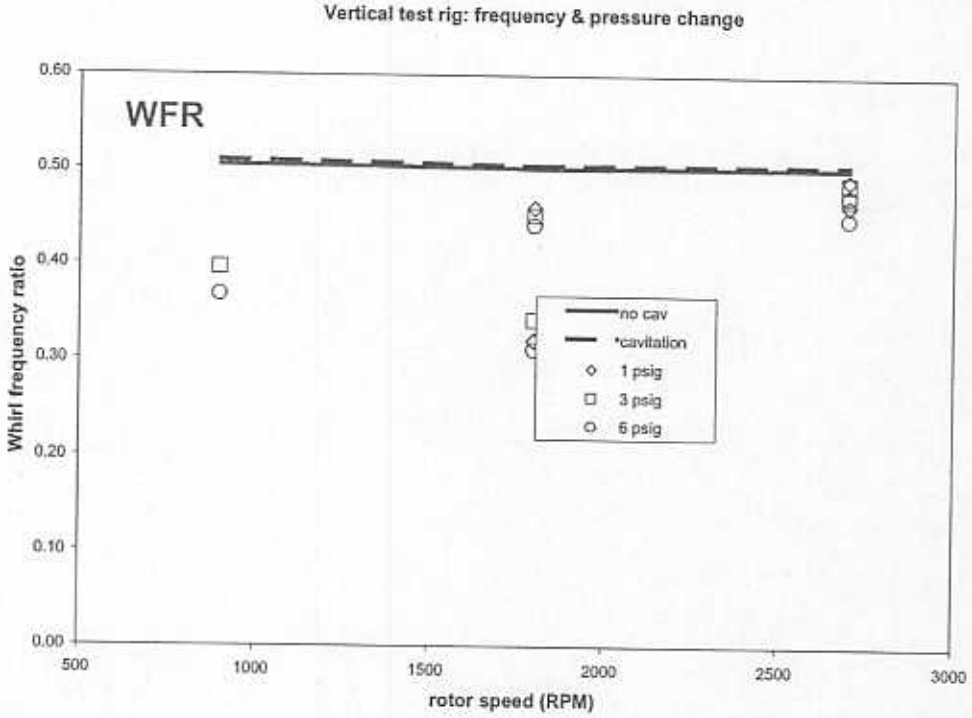

Figure 13 Experimentally estimated and predicted whirl frequency ratio vs rotor speed. Test data for three feed pressures and excitation frequencies (15, 30, 45 Hz)

Appendix A

Experimental data and single frequency fits for tests at 3 psig

The following figures display the experimental results obtained for tests conducted with a feed pressure of 3 psig and three rotor speeds (900, 1800 and 2700 rpm) and three excitation frequencies (15, 30 and 34 Hz). The graphs depict the excitation forces in two independent experiments, $|F_x| > |F_y|$ and $|F_y| > |F_x|$, and the ensuing bearing motions. The components of bearing motion with frequencies equal to the rotor speed (1X) and the excitation frequency are shown. In each test, bearing orbits are displayed. Note the accuracy of the single frequency analysis (curve fits) depicting the bearing motion. The actual operating parameters, hot radial clearance and film temperature, are noted. The graphs include the recorded eccentricities, dimensionless relative to the actual clearance.

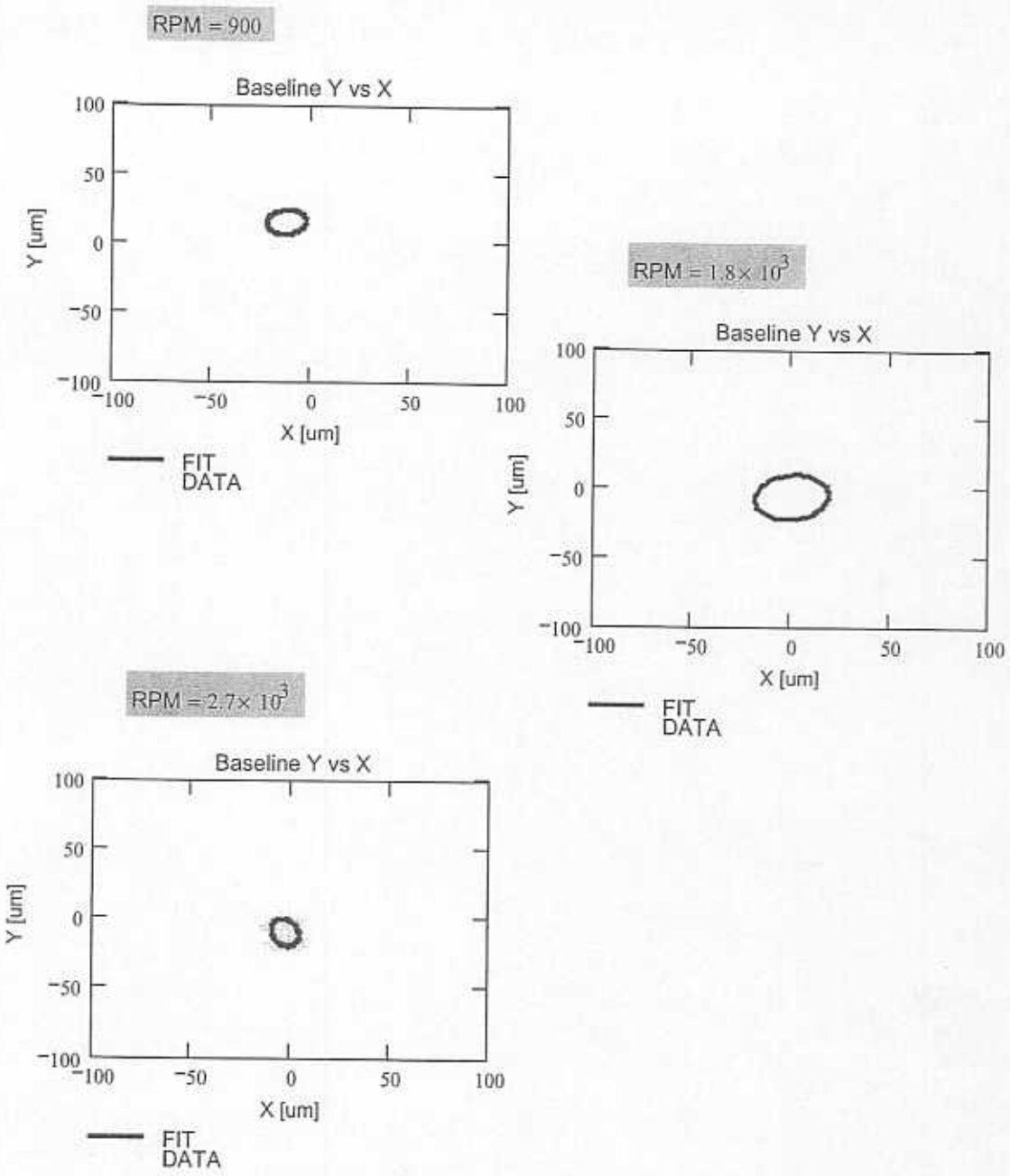

Figure A.1 Baseline (run out) rotor motion (no forced excitation) at rotor speeds of 900 rpm, 1800 rpm, and 2700 rpm. Feed pressure = 3 psig

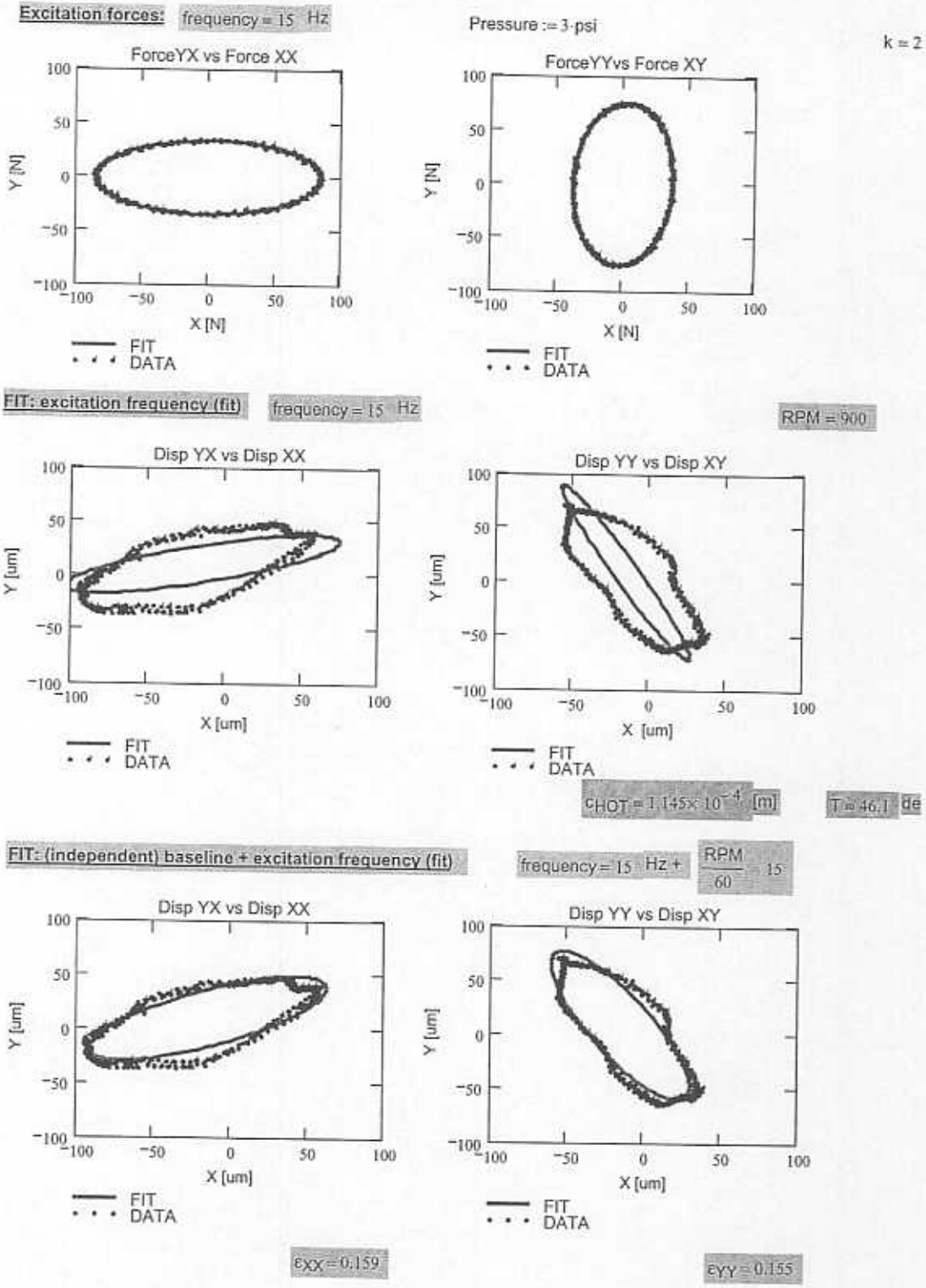

Figure A.2 Excitation forces (X,Y) and bearing dynamic responses for test at journal speed 900 rpm (15 Hz) and excitation frequency (15 Hz), feed pressure 3 psig. Top: Forces in [N]; Middle: Bearing motions (X,Y) in μm, data and excitation frequency component; Bottom: Bearing motions (X,Y) in μm, data and excitation plus synchronous journal speed components

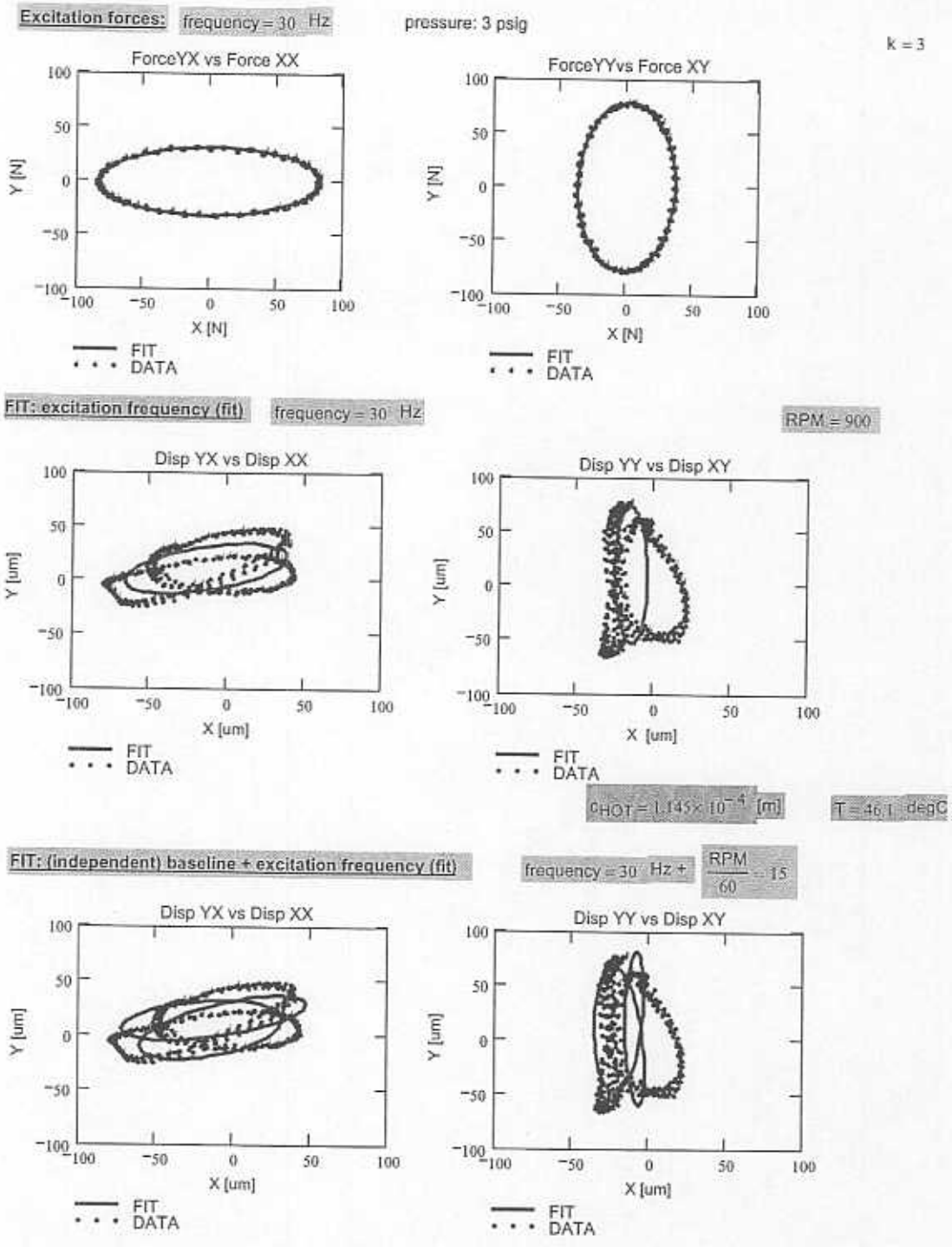

Figure A.3 Excitation forces (X,Y) and bearing dynamic responses for test at journal speed 900 rpm (15 Hz) and excitation frequency (30 Hz), feed pressure 3 psig. Top: Forces in [N]; Middle: Bearing motions (X,Y) in μm, data and excitation frequency component; Bottom: Bearing motions (X,Y) in μm, data and excitation plus synchronous journal speed components

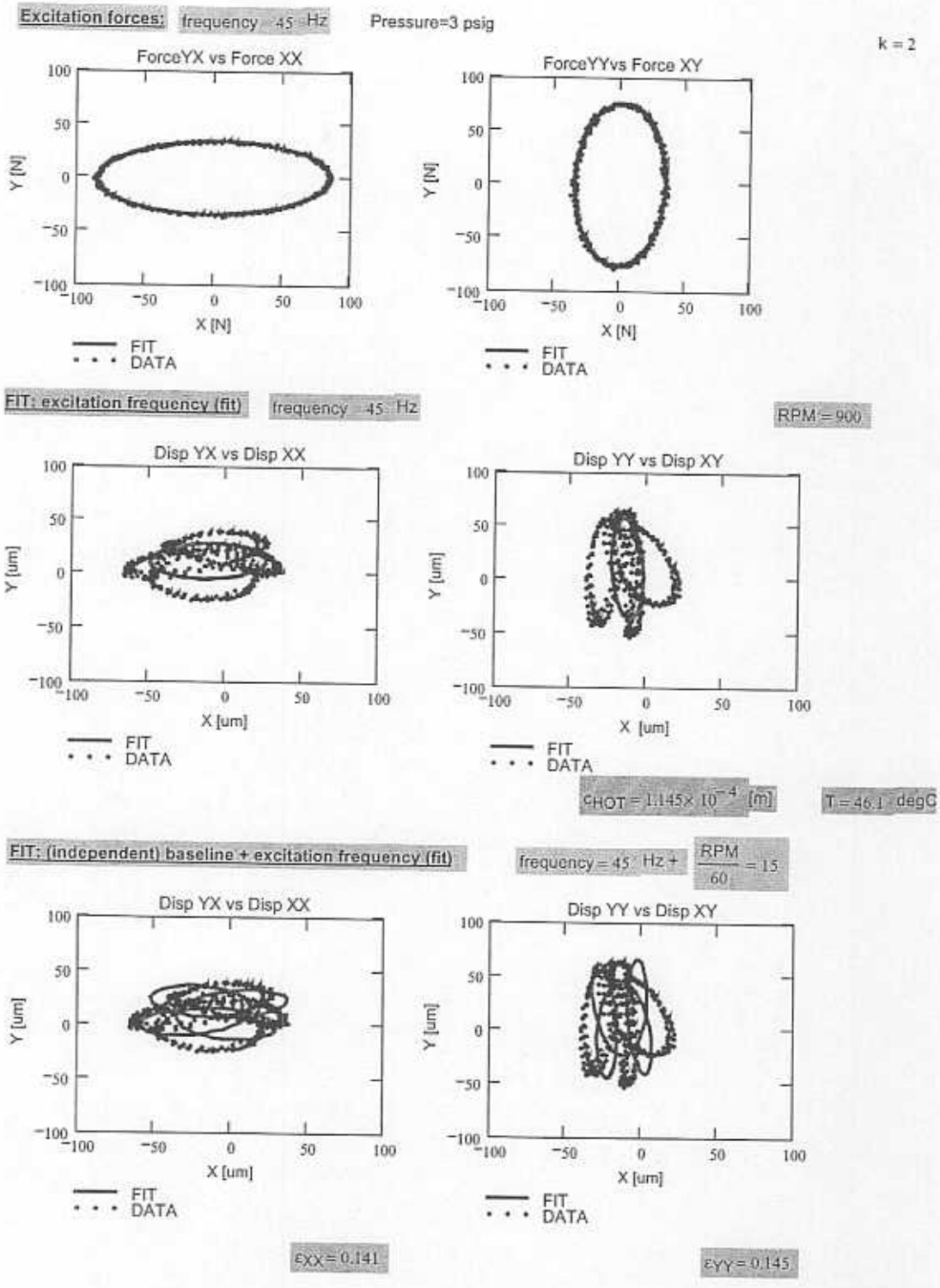

Figure A.4 Excitation forces (X,Y) and bearing dynamic responses for test at journal speed 900 rpm (15 Hz) and excitation frequency (45 Hz), feed pressure 3 psig. Top: Forces in [N]; Middle: Bearing motions (X,Y) in μm, data and excitation frequency component; Bottom: Bearing motions (X,Y) in μm, data and excitation plus synchronous journal speed components

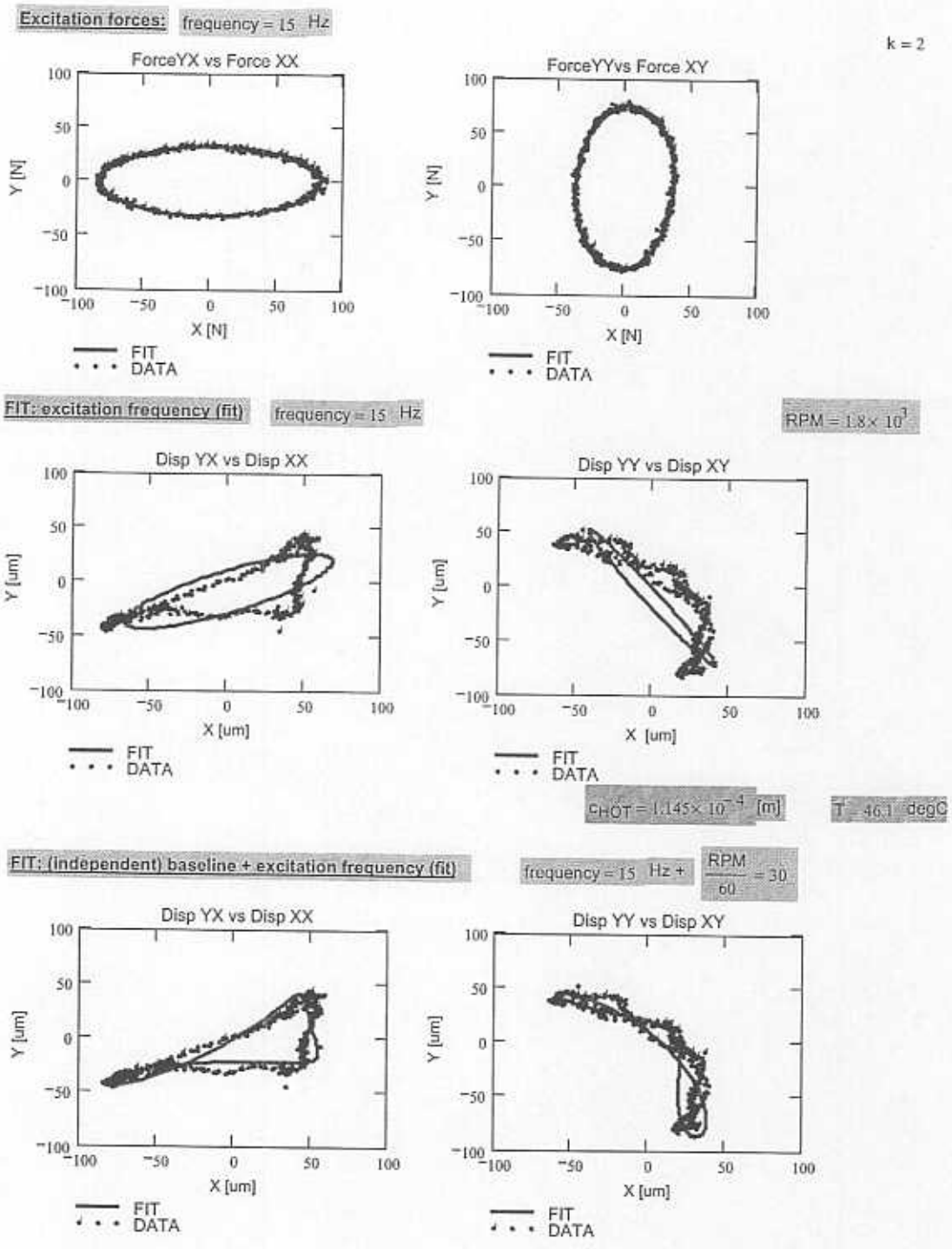

Figure A.5 Excitation forces (X,Y) and bearing dynamic responses for test at journal speed 1800 rpm (30 Hz) and excitation frequency (15 Hz), feed pressure 3 psig. Top: Forces in [N]; Middle: Bearing motions (X,Y) in μm, data and excitation frequency component; Bottom: Bearing motions (X,Y) in μm, data and excitation plus synchronous journal speed components

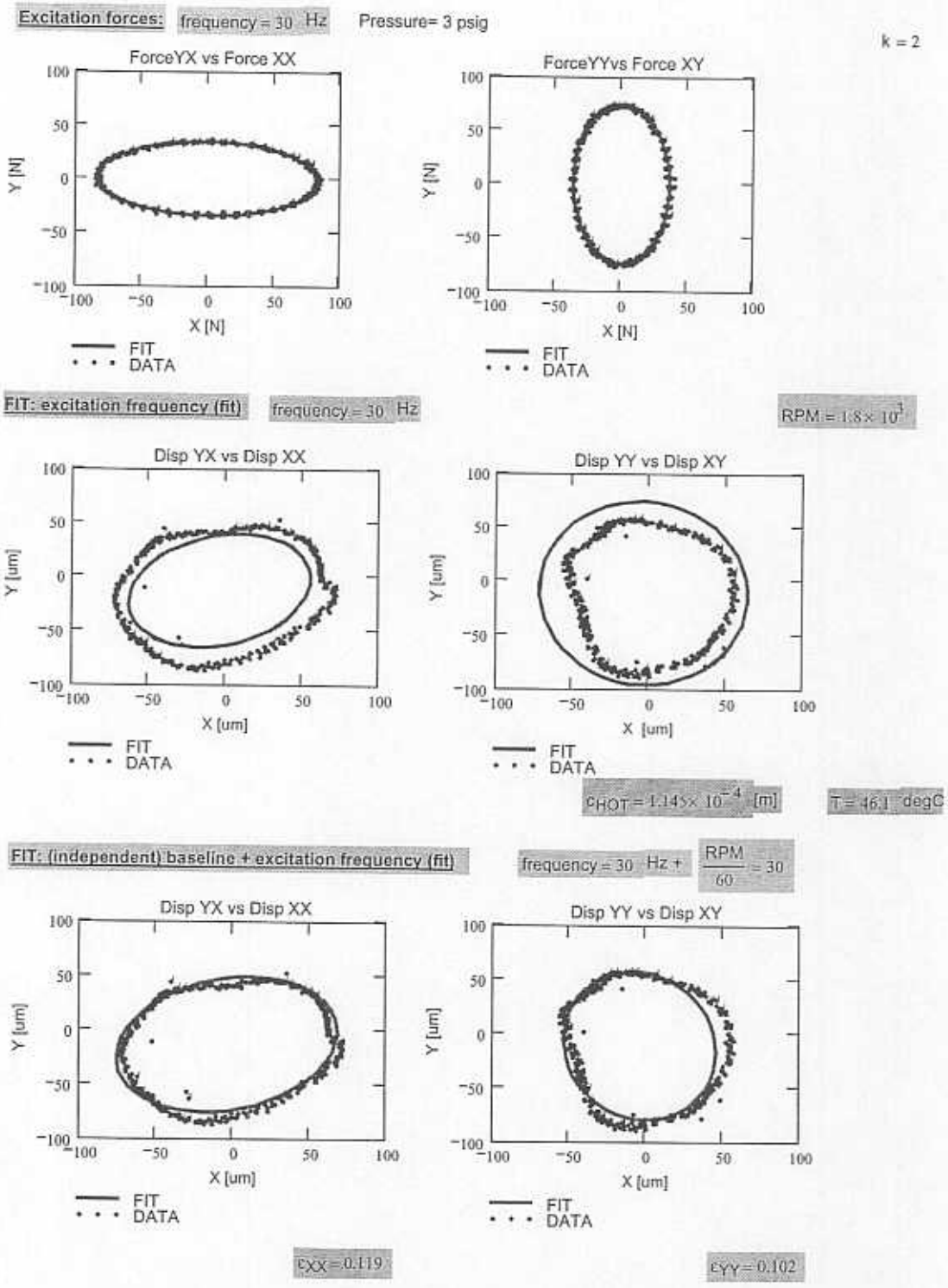

Figure A.6 Excitation forces (X,Y) and bearing dynamic responses for test at journal speed 1800 rpm (30 Hz) and excitation frequency (30 Hz), feed pressure 3 psig. Top: Forces in [N]; Middle: Bearing motions (X,Y) in μm, data and excitation frequency component; Bottom: Bearing motions (X,Y) in μm, data and excitation plus synchronous journal speed components

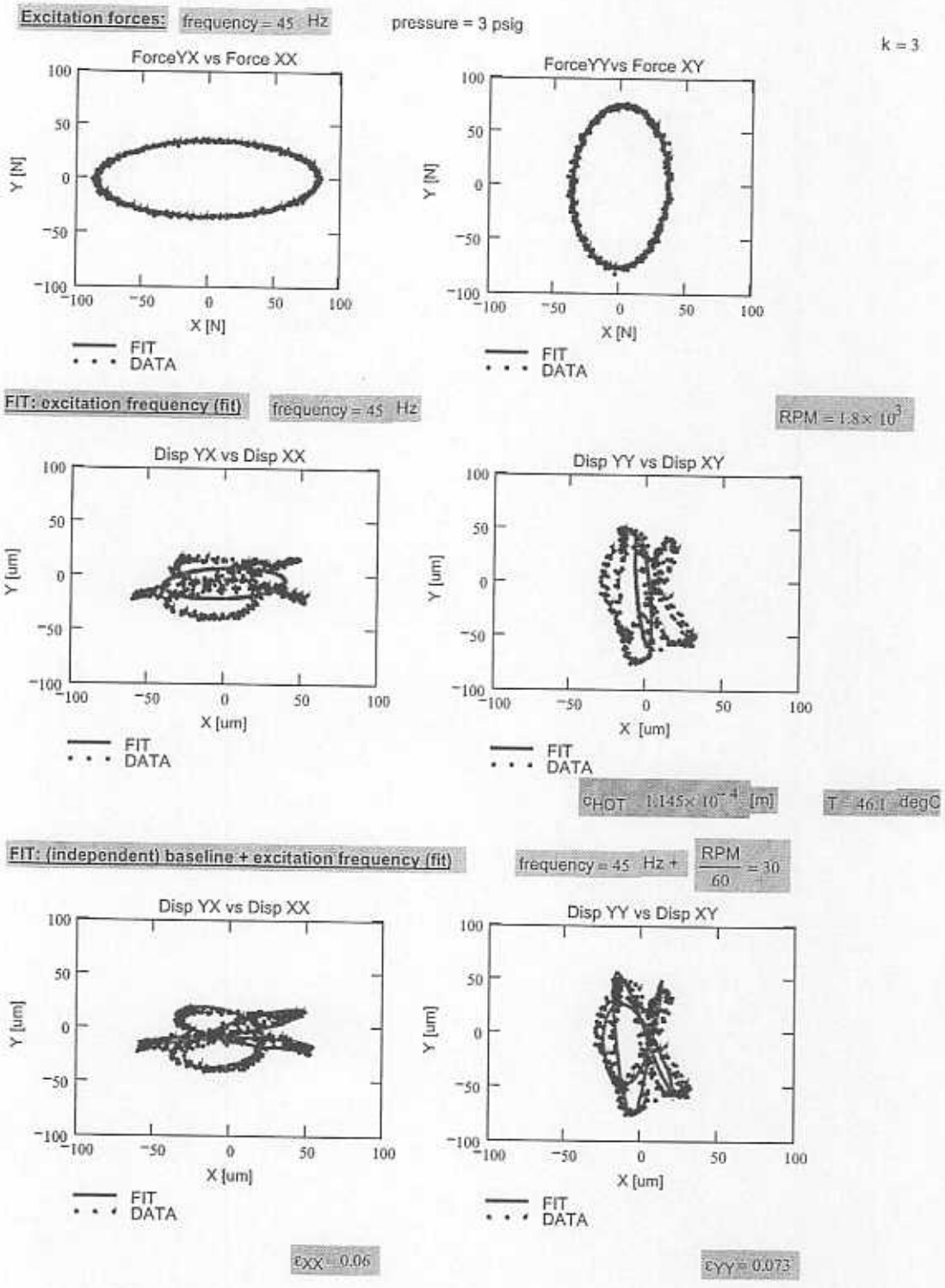

Figure A.7 Excitation forces (X,Y) and bearing dynamic responses for test at journal speed 1800 rpm (30 Hz) and excitation frequency (45 Hz), feed pressure 3 psig. Top: Forces in [N]; Middle: Bearing motions (X,Y) in μm, data and excitation frequency component; Bottom: Bearing motions (X,Y) in μm, data and excitation plus synchronous journal speed components

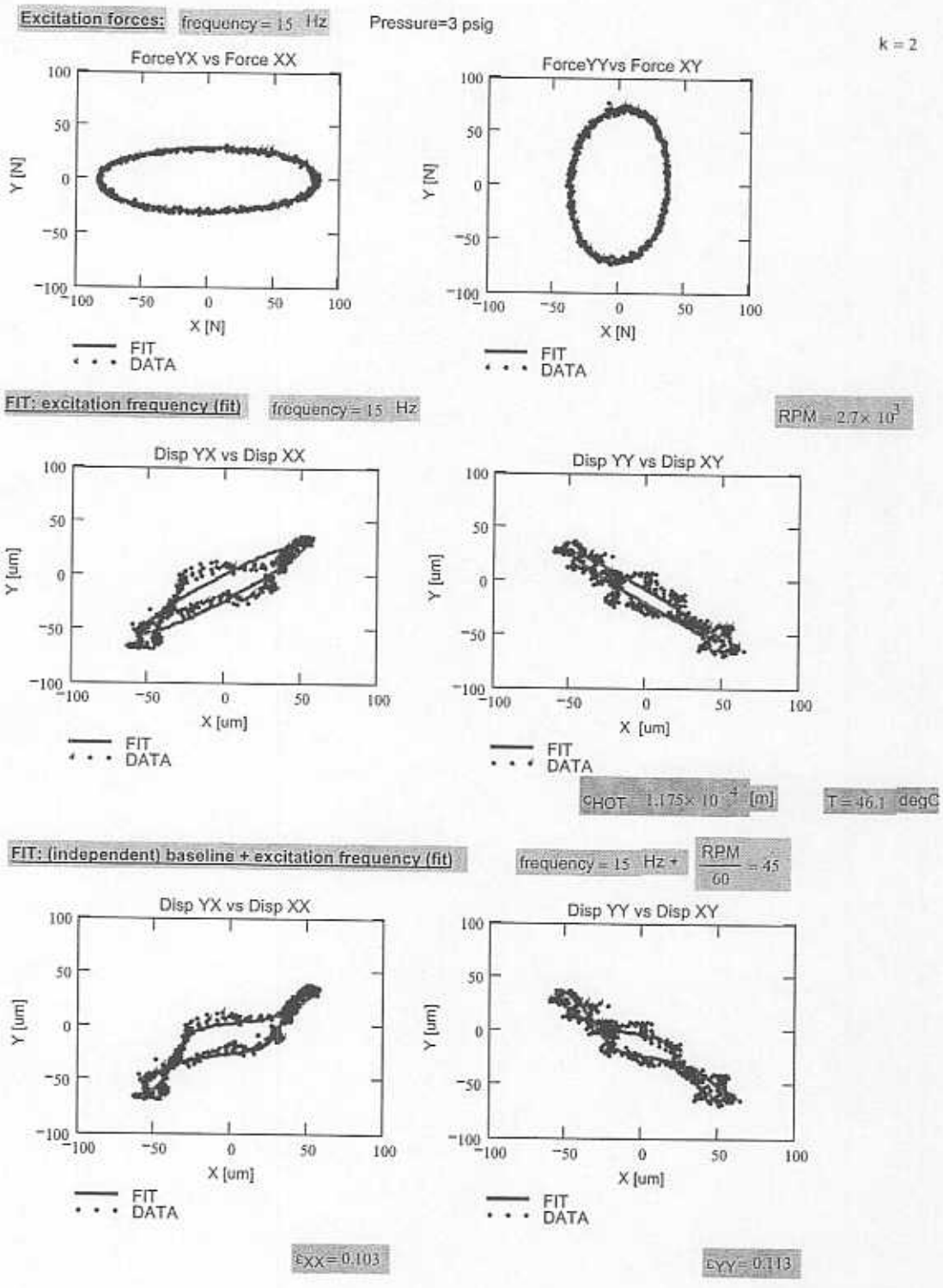

Figure A.8 Excitation forces (X,Y) and bearing dynamic responses for test at journal speed 2700 rpm (45 Hz) and excitation frequency (15 Hz), feed pressure 3 psig. Top: Forces in [N]; Middle: Bearing motions (X,Y) in μm, data and excitation frequency component; Bottom: Bearing motions (X,Y) in μm, data and excitation plus synchronous journal speed components

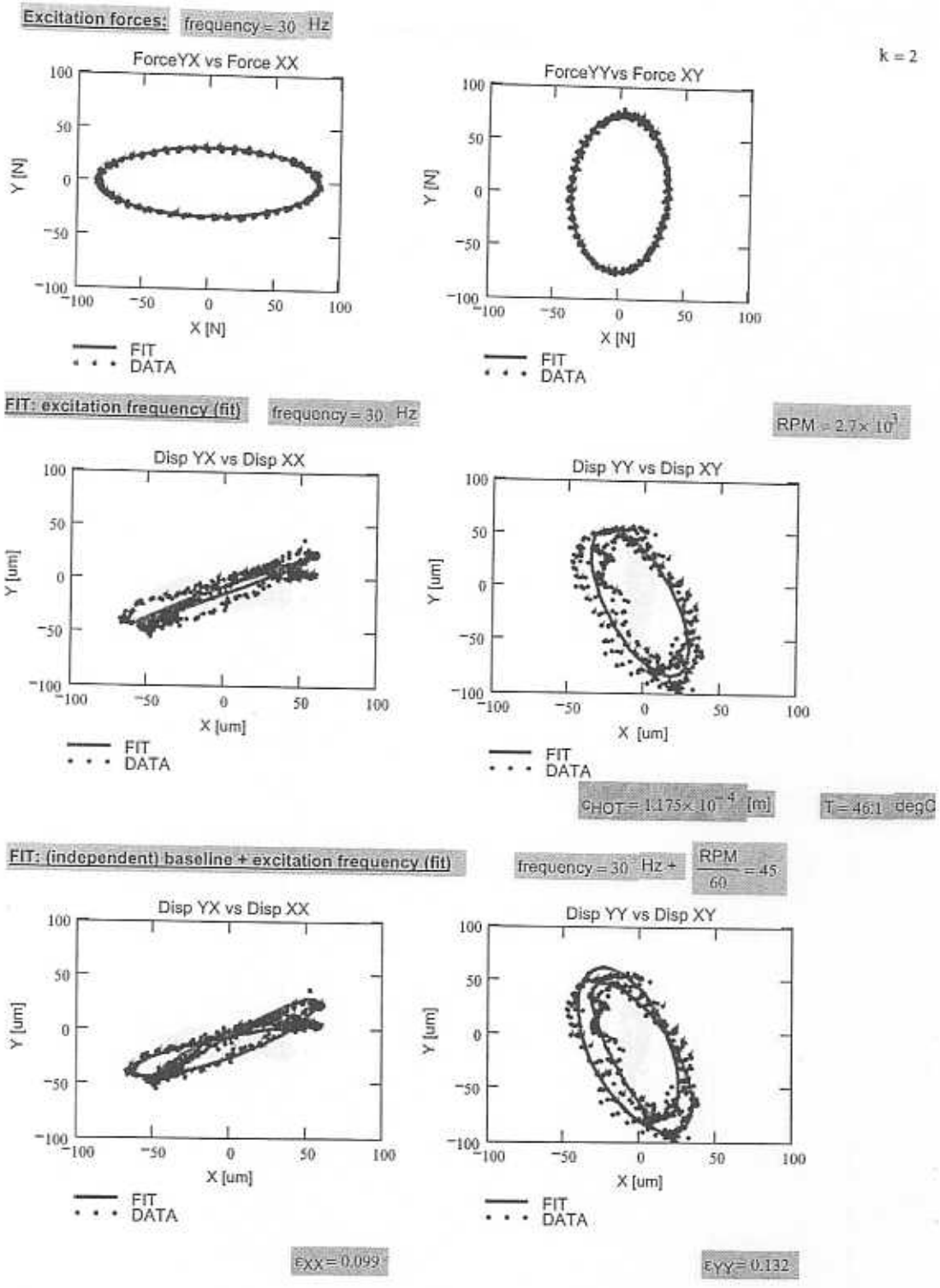

Figure A.9 Excitation forces (X,Y) and bearing dynamic responses for test at journal speed 2700 rpm (45 Hz) and excitation frequency (30 Hz), feed pressure 3 psig. Top: Forces in [N]; Middle: Bearing motions (X,Y) in μm, data and excitation frequency component; Bottom: Bearing motions (X,Y) in μm, data and excitation plus synchronous journal speed components